Utrecht Univeristy

Master thesis:

Using Surface Enhanced Raman Spectroscopy to study thin SURMOFs

Author:
Joris Koek

Supervisors:
R. P. Brand & prof. dr. ir. B.M.Weckhuysen

August 3, 2015

Abstract

Metal organic frameworks are an emerging class of highly porous materials with a great variety of potential applications. Recently surface anchored metal organic frameworks (SURMOFs) have been introduced. In this approach MOFs are grown in a layer-by-layer fashion which gives excellent control over their composition, orientation and thickness. In this research characterization of these SURMOFs is carried out using a new method utilizing surface enhanced Raman spectroscopy. A SURMOF substrate is covered with gold or silver nanoparticles and a Raman spectrum is recorded. This gives a huge increasement in the Raman signal obtained, which allowed us to measure the Raman spectra of very thin SURMOF layers. Using this technique we were able to see an increase in SURMOF thickness with subsequent growth cycles by observing a Raman signal intensity increasement. Surprisingly, after just one depistion cycles the MOF building blocks were already detectable on the substrate. Additionally, the shape of the Raman spectra allowed us to monitor the ratio of the different MOF building blocks which is indicative of the structure of the MOF. Consequently, the technique presented here shows great sensitivity and provides us with more chemical information than standard surface techniques like AFM.

Contents

1 Introduction

Surface Enhanced Raman Spectroscopy (SERS) is a spectroscopic technique that utilizes metal nano-corrugated surfaces to enhance a Raman signal [1]. SERS was discovered in the late 1970's on electrochemically roughened silver surfaces [2]. Since then, the field of Surface Enhanced Raman Spectroscopy has grown dramatically, being subject of 5000 research articles, 100 review articles and several books [3].

More recently shell-isolated nanoparticle-enhanced Raman spectroscopy (SHINERS) has been discovered [4]. In this approach the signal enhancing nanoparticles are coated with a inert metal oxide layer of only a few nanometers thick. Coating the metal nanoparticles has some advantages over using bare metal nanoparticles. First of all, the investigated substance does not adsorb on the metal surface. This has some advantages which will be discussed later in the theory section. Furthermore, the ultrathin coating stabilize the nanoparticles and keep them from agglomerating.

In this study we have utilized SERS to measure thin layers of Surface anchored Metal Organic Frameworks (SURMOFs). We are interested in the growth of SURMOFs that are grown in a layer-by-layer fashion. Techniques such as Surface Plasmon Resonance (SPR) [5], Quartz Crystal Microbalance (QCM) [6] and Atomic Force Microscopy (AFM) [7,8] have been used to study growth of metal organic frameworks. One big drawback of these techniques is that they do not give any chemical information about the sample. With SPR only average thickness of the SURMOF is measured, and with QCM only average increasement of thickness can be measured. With AFM morphology can be studied, but no chemical information is retrieved. By using SERS we hope to study thin SURMOF layers on a chemical level.

We have utilized noble metal nanoparticles deposited on thin films of Cu(ndc)(dabco)$_{0.5}$. The SERS effect gave us the signal enhancement needed to be able to detect SURMOF of only a few layers thick. We have used gold nanoparticles, silver nanoparticles and gold Shell Isolated Nanoparticles (SHINs) which were applied as colloidal suspensions in water. A schematic image of such a measurement is shown in figure 12.

A series of Cu(ndc)(dabco)$_{0.5}$ SURMOFs with different amount of immersion cycles was made. We are predominantly interested in the earliest growth stages, so samples with the following number of growth cycles were made: 1, 2, 3, 4, 5, 6, 8, 10 and 20. We have studied the possibility to detect MOF structure on the thinnest SURMOF samples. Additionally, Raman maps of the samples were measured to gain more insight in the coverage of these thin SURMOF samples in the earliest growth steps. AFM was used to study the morphology of the SURMOS samples.

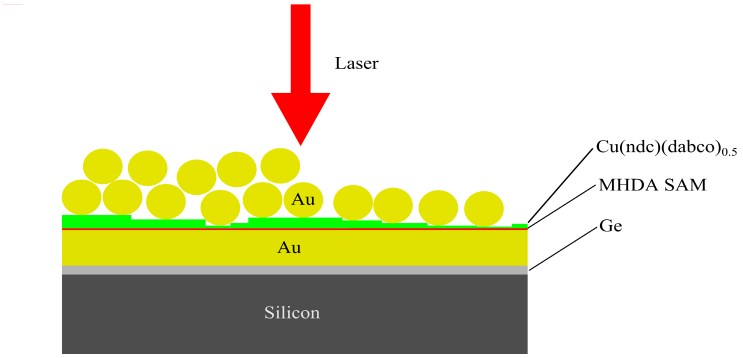

Figure 1: Schematic illustration of a SERS measurement of Cu(ndc)(dabco)$_{0.5}$ using gold nanoparticles.

2 Theory

2.1 Vibrations in molecules

As Raman spectroscopy is the main tool used in this research some basics of vibrational spectroscopy are introduced.

Vibrations in molecules are periodic motions of atoms in the molecule, the frequency of the periodic motion is known as a vibration frequency. Rotations can also be periodic motions but they are not considered vibrations because the centres of mass of the atoms in the molecule do not change position with respect to each other.

Molecular vibrations can be treated using Newtonian mechanics to calculate the correct vibration frequencies [9]. If the assumption is made that molecules can be approximated by masses connected with springs, and the force required to extend the spring is proportional to the extension (harmonic oscillator), the correct vibration frequencies can be calculated. In figure 2 such a system is illustrated.

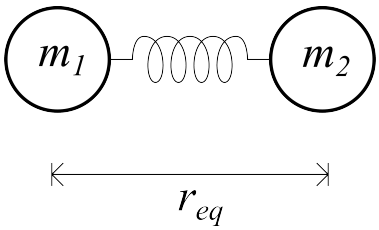

Figure 2: Illustration of a simple harmonic oscillator r_{eq} is the equilibrium distance between the masses, m_1 and m_2 are the masses of the atoms respectively.

The linear relation between force and extension for such a system is given by Hooke's law: equation 1.

$$F = -kx \tag{1}$$

With F the force, k the force constant and x the extension from the equilibrium distance. Next we consider Newton's second law: equation 2.

$$F = \mu \frac{d^2x}{dt^2} \tag{2}$$

Where μ is the reduced mass of the system, given by equation 3

$$\mu = \frac{m_1 m_2}{m_1 + m_2} \tag{3}$$

If we now equate (1) and (2) and divide by μ we come to equation 4, which is to be solved for x to calculate the vibration frequency.

$$\frac{d^2x}{dt^2} = -\frac{k}{\mu}x \tag{4}$$

The solution to this differential equation is given in equation 5.

$$x_t = x_0 \cos(2\pi\nu t); \quad \nu = \frac{1}{2\pi}\sqrt{\frac{k}{\mu}} \tag{5}$$

Where x_0 is the distance at $t = 0$, which is the most extended position. From equation 5 we conclude that the masses of the atoms and the bond strength between them determine

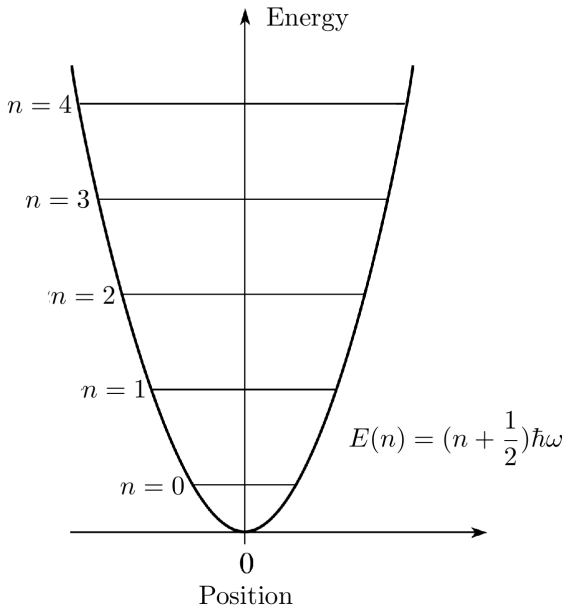

Figure 3: Illustration of a harmonic oscillator, the x-axis represents the position of one atom while the other atom is fixed. The y-axis represents the energy states with increments of $\hbar\omega$. When the system is excited, a transition from $n \rightarrow n + i$ occurs.

the frequency of the vibration. Therefore this frequency is unique and can be used to identify the molecule.

So by using classical mechanics the vibration energy of a simple diatomic molecule can be calculated. However, to get to a full description of the system quantum mechanics must be used. The general solution of the Schrödinger equation valid for this system leads to a sequence of evenly spaced energy levels characterized by a quantum number n: equation 6.

$$E(n) = (n + \frac{1}{2})\hbar\omega \tag{6}$$

If we plot the energy against the position of the atoms we obtain a schematic illustration of the harmonic oscillator, as illustrated in figure 3.

So far only simple diatomic molecules have been treated. In reality, however, most molecules are far more complex. In these molecules not only 1D stretch vibrations, but also 2D and 3D vibrations like bending modes are possible. The number of possible vibrations in a molecule is determined by the number of atoms in the molecule [9,10]. Every atom is able to move in three dimensions (x, y and z) and in principle every periodic movement of an atom can be considered a vibration. However, some of these movements result in a displacement of the whole molecule, which does not count as a vibration. The total number of vibrations is therefore given by $3N - 6$ (for non-linear molecules), in which N is the number of atoms in the molecule. For linear molecules the number of vibrations is $3N - 5$. In figure 4 the vibrations of CO_2 are depicted.

With vibrational spectroscopy transitions between the vibrational states illustrated in figure 3 are measured using electromagnetic radiation [9]. According to equation 5 transitions between these vibrational states occur at specific energies for specific bonds, giving chemical information about the substance. Hence, the interpretation of vibrational spectra involves the correlation of experimentally found absorption peaks with known absorption frequencies of certain types of bonds.

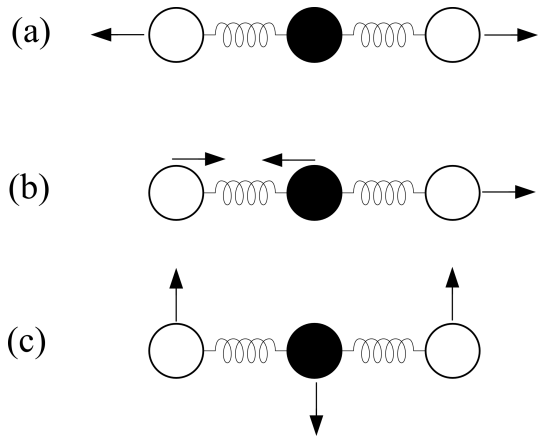

Figure 4: Possible vibrations of a CO_2 molecule. The bonds are represented as springs. (a) represents the symmetric stretch vibration, (b) is the asymmetric stretch vibration and (c) is the bending mode. There exists another bending mode but this one is degenerate with (c) due to symmetry.

2.2 Raman spectroscopy

Raman scattering is a spectroscopic technique in which vibrations in molecules are measured by analyzing their scattering of light. When light is scattered on substances most of the light is scattered elastically. Elastic scattering of light is called Rayleigh scattering: only the direction of the light is changed, the energy however, remains unchanged. In addition to elastic scattering there is also inelastic scattering, in which both the direction *and* the energy of the scattered light changes. The shift in wavelength corresponds to energies associated with transitions between rotational, vibrational and electronic states of the system [11]. Scattering of this type is called Raman scattering after the Indian physicist C. V. Raman who first observed this effect in liquids in 1928 [12,13]. There are two types of Raman scattering: scattering with a negative shift in energy which is called Stokes-Raman scattering and scattering with a positive energy shift which is called anti-Stokes Raman scattering.

In figure 5 the transitions associated with Rayleigh and Raman scattering are depicted [14]. On the left Rayleigh scattering is shown: the incident and scattered photons are of the same energy, this means no shift in wavelength is observed. In the middle Stokes Raman scattering is shown: the scattered photon is of lower energy than the incident photon. Part of the energy of the photon is transferred to the molecule which is now in a higher vibrational state: E_1. In this case the wavelength of the observed scattered light is longer. On the right Anti-Stokes Raman scattering is shown: the molecule already was in a higher vibrational state E_1, and the energy is transferred to the scattered photon. Scattered light with a shorter wavelength is observed. Consequently, by analyzing the energy of the scattered light the vibrational energies of molecules can be measured.

It should be noted that the majority of the radiation is scattered without change in wavelength: only 1 in 10 million photons are scattered via the Raman mechanism [15]. Most spectroscopic techniques use either absorption of radiation or emission caused by fluoresence, Raman spectroscopy is different in this sense since it is a spectroscopic technique based on scattering.

From figure 5 it is clear that Raman bands are not characterized by their absolute wavenumber, but rather by the shift in wavelength from the incident light. The shift in wavenumber, $|\Delta\tilde{\nu}|$ is usually referred to as the Raman shift, this is usually the quantity plotted on the x-axis in Raman spectra. In most experiments Stokes Raman scattering is used. Anti-Stokes Raman scattering is a temperature dependent process as the population

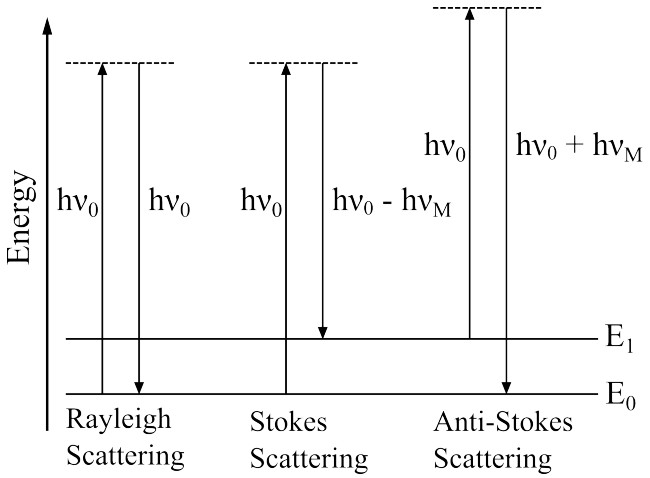

Figure 5: On the left Rayleigh scattering is shown; the incident and scattered photons are of equal energy. In the middle Stokes scattering is shown, the scattered photon is of lower energy. On the right anti-Stokes scattering is shown, the scattered photon is of higher energy.

of higher vibrational states is dependent on temperature following a Boltzmann distribution. This type of measurement is used far less frequently than its Stokes counterpart [14].

There are certain selection rules that determine which transitions will participate in Raman scattering. For a vibration to be Raman active the polarizability must change [14]. The polarizability is the tendency of the molecule to become polarized when an external field is applied. The selection rules are different from IR spectroscopy were a transition is allowed if the dipole moment changes. This is the reason why IR and Raman spectroscopy are complimentary techniques: according to the selection rules they can measure different vibrations. For example molecular nitrogen does not have a dipole moment which means it shows no IR active vibrations, it does however have a considerable polarizability which means it does show Raman active vibrations. In figure 6a theroretical raman and IR spectra of gaseous CO_2 are shown.

In practise most spectra are measured in the liquid or solid phase. In the condensed phases the molecules have interactions with each other, which influence the IR and Raman spectra. For example in crystals, due to the interaction between neighboring molecules the symmetry can be slightly distorted [14]. The symmetry of a molecule in the crystalline phase is referred to as the site symmetry. Because the site symmetry can be different, vibrations can become active which would otherwise be inactive, as can be seen in figure 6b. This is just one effect concerning environment which influences the IR and Raman spectra measured: there are many more effects which cause peaks to split, broaden or shift. These effects are reasons why interpretating IR and Raman spectra can be rather difficult [15].

2.3 Surface Enhanced Raman Scattering

With Surface Enhanced Raman Scattering (SERS) metal nanostructures are used to enhance the Raman signal [16]. There are several mechanisms which contribute to the enhancement of the Raman signal, however, the exact mechanisms and their contribution to the SERS effect are still subject of debate [17]. SERS measurements are performed much in the same way as regular Raman measurements, the only difference being the use of metal nanostructures. The total SERS enhancement is said to be in the order of $10^{10} - 10^{11}$ [18–20].

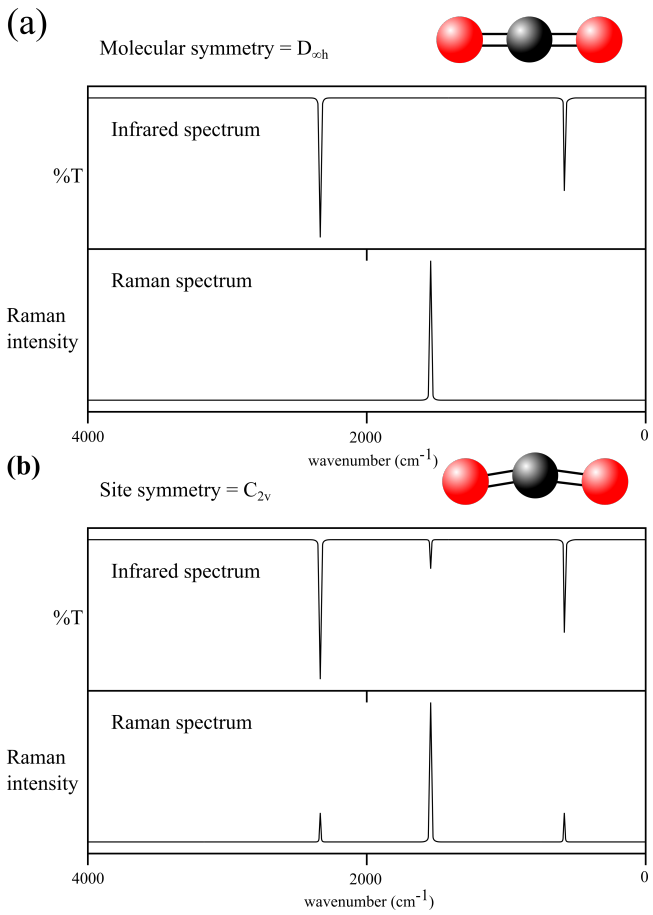

Figure 6: Theoretical infrared and Raman spectra of gaseous (a), and crystalline (b) CO_2 are depicted. Only vibrations are considered, rotations are not taken into account. As can be seen in (b) due to change in symmetry caused by the crystal, vibrations become active which would otherwise be inactive.

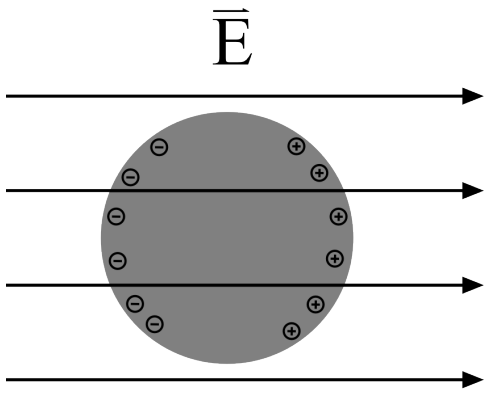

Figure 7: Metal sphere in an electric field, resulting in displacement of the free electrons in the metal. If the electric field is switched off the electrons will return to the right side. The electrons can then oscillate back and forward with a frequency characteristic for the metal and size of the nanoparticle.

2.3.1 Electric field enhancement effect

When nanostructures of certain metals are irradiated with light, a collective oscillation of the conduction electrons at the surface of the structure is generated [21]. This effect is called surface plasmon resonance. These electromagnetic surface waves arise via the coupling of the electromagnetic field of the incident light to oscillations of the conduction electrons in the metal.

Plasmons can be described in the classical picture as an oscillation of free electron density with respect to the fixed positive ions in the crystal. To visualize a plasmon oscillation, imagine a sphere of metal placed in an external electric field pointing to the right, as depicted in figure 7. Electrons will move to the left side (resulting in positive metal ions on the right) until they cancel the field inside the metal. If the electric field is removed, the electrons move to the right, repelled by each other and attracted to the positive ions on the right side. The electrons can then oscillate back and forth at a certain frequency, which happens to be in the visible light region for gold and silver. This strongly simplified explanation describes the dipolar plasmon resonance mode: the electric field around the metal nanoparticle follows that of an oscillating electric dipole. Higher harmonics are also possible, for example the quadrupolar resonance mode is also observed in metal nanoparticles [22].

Due to these surface plasmon resonances, a strong enhancement of the electric field close to the surface of the particles is generated. The metals for which this effect is most easily observed are gold, silver and copper. These surface plasmons are only localized when the metal strucures are sufficiently small. The bulk metals do not experience this field enhancement because their surface plasmons are propagating. However, in a small particle the waves are localized.

Since the Raman signal is proportional to $|E^4|$, a small increase in the local electric field already causes a great signal enhancement. Figure 8 depicts a simulation of the electric field

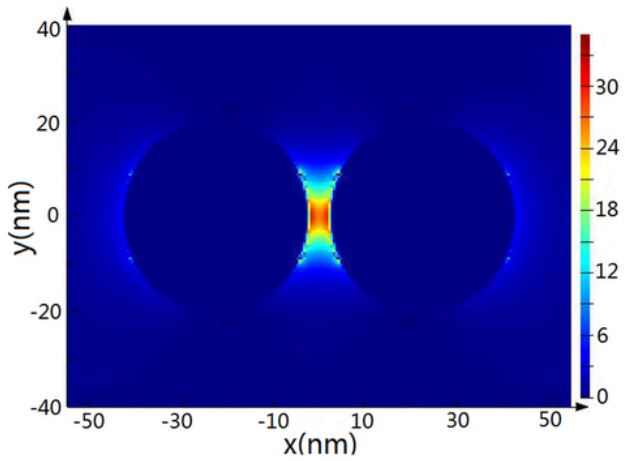

Figure 8: Intensity $\langle \mid E \mid^2 \rangle$ distributions obtained from 3D FDTD calculations at wavelength 633nm of silver nanoparticles, with 40nm diameter and interparticle separation of 5nm on a silicon wafer. As can be seen in the figure in between the particles the electric field is enhanced very strongly. The enhancement factor on the left is scaled to the magnitude of the electric field of the incoming light. Taken from [23].

around silver nanoparticles illuminated with a laser [23]. As can be seen in the figure a very strong enhancement of the electric field is present in between the particles. If a molecule would be located on such a hot spot it would experience a very strong signal enhancement, due to the relatively high electric field at that position.

As illustrated in figure 8 it is very benificial to bring such metal nanostructures close to each other, since creating these SERS hot spots will result in large signal enhancements. A lot of research on SERS is focused on creating nanostructures which contain SERS hot spots such as dimers and trimers [24], nanostars [25] and nanoparticle dimer arrays [26]. Usually the electric field enhancement effect gives the largest contribution to the overall SERS enhancement [16].

2.3.2 Chemical enhancement effects

There are several effects which can contribute to the chemical enhancement of a Raman signal [27]. For chemical enhancement effects to take place the molecules must be adsorbed on the metal surface of the enhancing particle [28]. It is therefore clear that in the case of multilayer adsorption only the first monolayer will experience the chemical enhancement effects. A possible mechanism for signal enhancement is excitation of the molecule via a charge transfer mechanism, this effect is illustrated in figure 9. In the charge transfer mechanism the molecule is excited by interaction with the metal energy states [28]. Upon adsorption a metal substrate complex is formed. If the Fermi level of the metal is in between the HOMO and the LUMO of the molecule, charge transfer between molecule and metal is possible. By providing an additional pathway for excitation the chance of Raman scattering taking place is increased [28].

Another mechanism which can enhance signals or even activate vibrations is simply induction of a change in the symmetry of the adsorbed molecule. Symmetry predominantly determines which vibrations are observed in Raman and IR spectra. If the symmetry of the molecule is changed upon adsorption the molecule might show vibrations which would normally not be seen. This effect is especially eminent if the molecule has a strong affinity for the metal surface, since then a strong bond is formed which may distort the molecular symmetry [28].

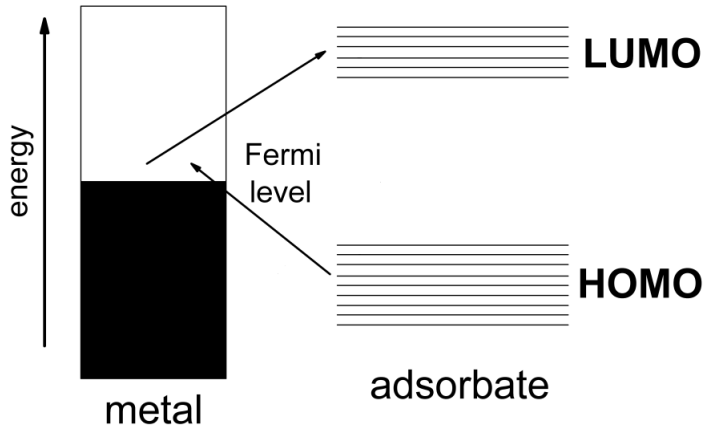

Figure 9: Energy levels of the adsorbate and the metal are shown. Excitation can take place via interaction with the metal energy states(charge transfer mechanism), or the molecule can be excited directly.

Conclusively, the described chemical effects intrinsically change the observed Raman spectrum, because parameters like the energies of the HOMO and LUMO and symmetry play a role. Therefore, unlike the electric field enhancement described earlier, chemical enhancement is always molecule specific. Consequently, the electric field effect predominantly determines the strength of the signal and therefore the signal to noise ratio, and the chemical effects determine the shape of the actual SERS spectrum l [27].

2.4 SERS substrates

Colloidal metal nanoparticles deposited on glass or silicon are ideal substrates for SERS measurements, due to their low cost, ease of preparation, chemical stability and large SERS signal enhancement [29]. The easiest and most widely used method to produce metal nanoparticles is the reduction of the corresponding metal precursor in aqueous solution. This method will yield a colloidal suspension with the metal nanoparticles of the desired size. Generally the size regime relevant to SERS experiments is between 10 and 80 nm [27].

2.4.1 Gold nanoparticles

The most common synthesis of gold nanoparticles is the standard citrate reduction method, based on the work of Frens [30]. In this approach 100 mL of a 0.1% solution of chloroauric acid is reduced with a 1% trisodium citrate solution. The citrate acts both as a reducing agent and as a ligand to the gold particles in this reaction. This means that by adding more citrate there will be more gold-water interface stabilization, resulting in smaller particles. Additionally the pH is also influenced by the amount of citrate, this also has an influence on the particle growth [31]. In table 1 the size of the nanoparticle as a function of the amount of sodium citrate added is given. It is very important that this reaction is carried out in an enviroment free of other metal ions, so purified water (mQ) must be used.

As with any nanoparticle synthesis control over the nucleation step is very important. From the precursor, atomic monomers are formed. If the concentration of monomers exceeds their natural solubility (supersaturation) nucleation will start, forming small nuclei which will grow [32]. However, growth will only take place if the total free energy of the system lowered. In equation 7 the formula for the free energy change of the system as function of particles radius is given.

Table 1: Nanoparticle size as a function of amount of 1% sodium citrate solution added to 100 mL of 0.1% $HAuCl_4$. Reproduced from [30].

Amount 0.1 % sodium citrate added (mL)	Nanoparticle diameter (nm)	Color
2.0	16.0	Orange
1.5	24.5	Red
1.0	41	Red
0.6	71.5	Dark red
0.42	97.5	Violet
0.32	147.0	Violet

$$\Delta G = \frac{4}{3}\pi r^3 \Delta g + 4\pi r^2 \sigma \tag{7}$$

Where ΔG is the free energy of the system, Δg is the difference in free energy per unit volume between the liquid phase and the solid phase, r is the radius of the particle and σ is the interfacial energy. Δg can also expressed in terms of supersaturation, equation 8.

$$\Delta g = \frac{\Delta \mu}{v} = \frac{kT}{v}\, ln(\alpha); \quad \alpha = \frac{C_{ss}}{C_s} \tag{8}$$

Where $\Delta \mu$ is the difference in chemical potential between the dissolved monomers and the nucleated solid phase, v is the volume of one monomer, k is the Boltzmann constant and T is the temperature. The supersaturation ratio, α is expressed as the ratio between the supersaturation C_{ss}, and the concentration of a saturated solution C_s. In figure 10 equation 7 is plotted. The creation of surface is the energy positive term which increases quadratically and the decrease of chemical potential is the energy negative term which increases cubically. To allow nucleation to take place the energy barrier needs to be passed, this can be done by increasing the supersaturation or by introducing seeds in the system [33]. In the case of gold nanoparticle synthesis with the Frens method the injection of citrate creates a sudden burst of monomers, which dramatically increases the supersaturation, this allows nuclei to form [32]. Ideally nucleation only takes place once, followed by growth, this will result in the most monodisperse particles. However, it is very hard to realize this, because there might be pre-existing nucleation points like other metal ions in the solution. Also small nanoparticles may meet and aggregate in the initial stages which may lead to non spherical particles. Frens' method gives monodisperse particles because by injecting a small amount of citrate in the already boiling chloroauric acid solution, the duration of the nucleation stage is minimized [30].

2.4.2 Silver nanoparticles

Silver nanoparticles are made in a similar way to gold nanoparticles. The most commonly used synthesis method was developed by Lee and Meisel [34]. In this approach silver nitrate is reduced by sodium citrate and silver nanoparticles are formed. The nucleation and growth mechanism described above is similar for silver nanoparticles. One big difference however is that silver is much easier oxidized. The oxidation of the silver in the early stages of the synthesis leads to less spherical particles with a bigger polydispersity. Because silver nanoparticles oxidize much faster, it is important to do the SERS measurements within a few days after synthesis, as SERS activity decreases dramatically after oxidation.

2.4.3 Shell isolated gold nanoparticles (SHINs)

Although gold and silver nanoparticles are good SERS substrates, sometimes more advanced systems are required for performing good measurements. In certain cases the fact that the

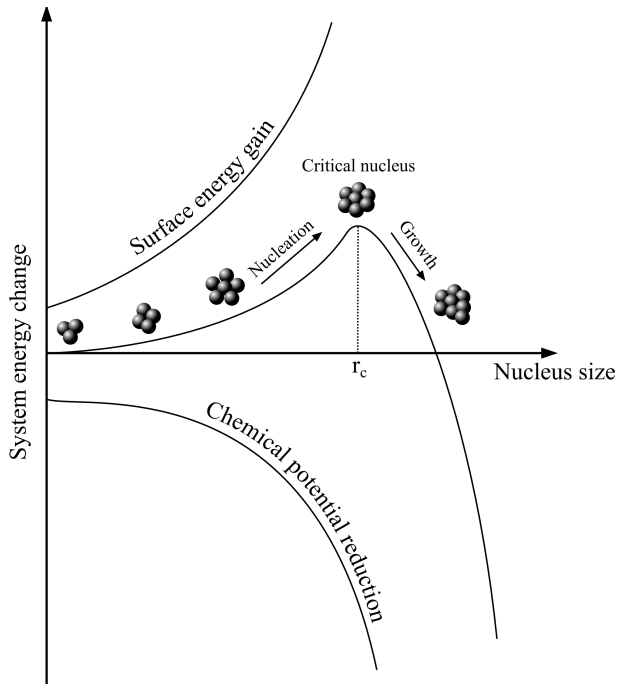

Figure 10: Schematic plot of equation 7. The particle radius is plotted against the free energy change of the system. When a certain critical radius is exceeded, particles can grow because then the slope of the curve becomes negative.

molecules of interest physically adsorb on the metal surface influences the measurement itself. It might be preferential to take advantage of the electric field effect, but to exclude the chemical effects. To realize this, a thin shell of inert insulating material can be grown around the metal nanoparticles [4,35]. This layer should be free of holes as no metal surface available for adsorption can be exposed, since this would allow for chemical effects. Additionally it should be thin enough to allow the electric field enhancement to be present outside the particle. The enhancement of the electric field only protrudes several nanometers from the metal surface [23]. So a silica layer thinner than 3 nm is desired.

The first successful synthesis of such a system was realized by Liz-Marzan and coworkers [36], although it was not used for Raman measurements by them. Silica normally does not nucleate on the gold surface because of the big interfacial energy. However, if the gold nanoparticles are coated with (3-aminopropyl)trimethoxysilane (APTMS), the gold is functionalized with free Si-OH groups attached via a small amino alkane coordinated to the gold. The APTMS functionalized nanoparticles are then coated with silica by adding an acidified solution of sodium orthosilicate. The SHINs formed this way have a uniform pinhole free silica layer of tuneable thickness. By adjusting parameters like basicity and reaction time the silica thickness can be tuned. The deposition of silica onto the particles is strongly dependent on pH [37]. If the pH is too high the solubility of silica is too high and no deposition will take place. If the pH is too low silica will deposit too fast leading to thicker shells.

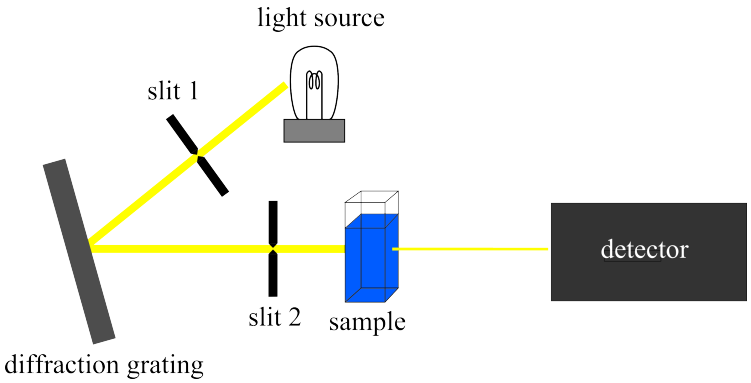

Figure 11: Schematic illustration of a UV-vis spectrometer.

2.5 Analysis techniques

2.5.1 UV-vis spectroscopy

UV-vis spectroscopy refers to absorption spectroscopy in the ultraviolet-visible spectral region [38]. With UV-vis spectroscopy the absorbance of the sample is scanned over a range of wavelengths. The range of wavelengths UV-vis spectrometers typically cover is 190-1100 nm. In figure 11 a schematic illustration of a typical UV-vis spectrometer is depicted. The setup consists of a light source which is usually a xenon lamp for the visible area, and a deuterium arc lamp for the UV part of the spectrum. A slit selects a single light beam which hits the diffraction grating. The diffraction grating diffracts the beam, and light with different wavelengths is diffracted under various angles. A wavelength is selected by using a second slit, by rotating the grating the desired wavelength is transmitted through the slit. In this way the absorption of the sample can be measured for different wavelengths. Gold and silver nanoparticle dispersions absorb light in the visible spectrum, this makes UV-vis spectroscopy a fast and easy characterization method for these systems.

2.5.2 Transmission electron microscopy

Because of the diffraction limit it is impossible to images particles smaller than the wavelength of light with conventional optical microscopy. A method to circumvent this is by using radiation with a shorter wavelength, for example electrons. Transmission electron microscopy (TEM) is a microscopy technique in which a beam of electrons is transmitted through a thin specimen [39]. Since the percentage of electrons absorbed or scattered by the material depends on its thickness, a 2D projection of the material is made as the electrons pass through. We are interested in the size and shape of the gold and silver nanoparticles as these parameters determine the SERS properties. As the nanoparticles are smaller than 100 nm, electron microscopy is the only method to directly image them. Additionally TEM can be used to image the thin silica shell on the SHINs.

2.5.3 Atomic force microscopy

Atomic force microscopy (AFM) is technique which utilizes a cantilever with a sharp tip to scan a specimen surface [40]. The tip radius of curvature is typically in the order of nanometers. When the tip is brought close to the sample surface, forces between the tip and the sample result in a deflection of the cantilever. This deflection is indirectly measured by detecting the deflection of a laser beam on the back of the cantilever. When the cantilever moves only slightly the laser beam angle is changed, by using a long beam path this small change is amplified. By scanning the sample surface a height map of the sample can be made.

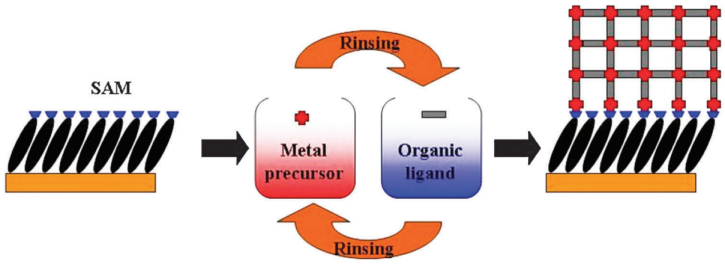

Figure 12: Schematic diagram for the step-by-step approach for the growth of the MOFs on substrates functionalized with SAMs. The approach is done by repeated immersion cycles first in solutions of the metal precursor and subsequently in the solution of organic ligand, after rinsing with the solvent in between. Taken from [43]

One of the most freuqently used modes of operation is the tapping mode. In this mode the cantilever is oscillated at its resonance frequency, when forces act on the tip the amplitude is changed and this can be measured by the beam deflection mechanism. AFM offers excellent resolution typically in the order of nanometers, which makes it a useful technique to study surfaces. This makes AFM the ideal tool to study the surface of the SURMOFs.

2.6 Surface anchored metal organic frameworks

Metal Organic Frameworks (MOFs) are an emerging class of highly crystalline porous materials constructed from metal containing nodes, and organic linker molecules. Due to the almost endless possibilities in structure and functionality, the area of MOFs has become one of the fastest growing fields in chemistry [41]. Lately intensive research has been done on fabrication of thin MOF films of a few µm thick, for potential applications such as catalysis, optoelectronics and gas separation [42,43].

A way to produce a thin layer of MOF material surface is the the layer-by-layer (lbl) deposition methods which was first utilized by Shekhah et al. [44]. This synthesis method leads to highly ordered, oriented MOF coating exhibiting crystalline order both perpendicular and parallel to the substrate surface. The lbl process consists of subsequent immersion steps in solutions containing the appropriate building blocks. In between each immersion step the substrate is washed with solvent and dried to remove any residual reactants. As substrates usually gold is used with a self assembled monolayer (SAM) of thiol molecules which have a functionality similar to one of the MOF building blocks. This way, a link is formed between the substrate and the MOF. A schematic representation of this procedure is shown in figure 12.

$Cu(ndc)(dabco)_{0.5}$ is a MOF consisting of 1,4-naphthalenedicarboxylate (ndc) coordinated to copper ions. Four ndc molecules coordinate to one pair of copper ions forming paddlewheel like structures. These paddlewheel like structures are connected with the nitrogen containing dabco pillars, which coordinate axial to the copper ion pair. In figure 13 the structure of $Cu(ndc)(dabco)_{0.5}$ is depicted.

$Cu(ndc)(dabco)_{0.5}$ can be grown with two different orientations. When a SAM of MHDA is used, carboxylic acid groups are exposed, and the [100] direction is promoted (the dabco pillars are oriented parallel to the gold surface). It should be mentioned however, that only the precursor addition order: $Cu(OAc)_2 \rightarrow H_2ndc \rightarrow$ dabco yields the crystalline SURMOF oriented in the [100] direction [6]. For the reverse linker sequence $Cu(OAc)_2 \rightarrow$ dabco $\rightarrow H_2ndc$ less crystalline material in the [100] orientation is obtained. The other orientation, in which the dabco pillars are oriented perpendicular to the surface ([001]), can be obtained by using a SAM of [4-(4-pyridyl)phenyl]methanethiol (PBMT) which mimics the dabco pillars. Remarkably, in this case the best results are obtained when adding the

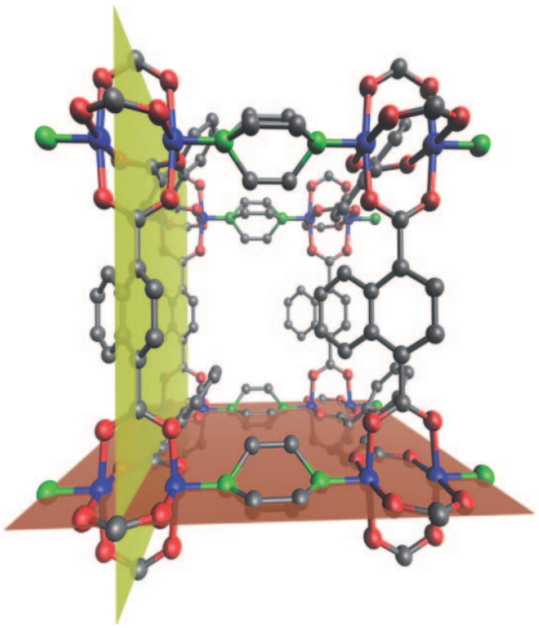

Figure 13: Schematic diagram of the Cu(ndc)(dabco)$_{0.5}$ stucture. When a MHDA SAM is used the growth direction of the MOF will be as indicated by the red plane. This is due to the carboxylic acid groups which mimic the ndc. Taken from [6]

ligands simultaneously.

Since we will apply our nanoparticles in water, it is important to consider the water stability of Cu(ndc)(dabco)$_{0.5}$. It is known from literature that certain MOFs are not resistant to water such as HKUST-1, which loses crystallinity almost completely after 12h of exposure to water vapour at 323 K [45]. However, Cu(ndc)(dabco)$_{0.5}$ should be more resistant to water as the hydrophilic copper ions are fully coordinated with ligands [46,47]. This means that the hydrophilic copper ions are completely blocked of by the hydrophobic ligands: ndc and dabco. No study on water stability of Cu(ndc)(dabco)$_{0.5}$ could be found in literature. However, MOFs similar to Cu(ndc)(dabco)$_{0.5}$ showed moderate stability to water vapour [47]. For example Zn(bdc)(dabco)$_{0.5}$ which is fairly similar to Cu(ndc)(dabco)$_{0.5}$ showed no significant water adsorption up to relative pressures of 0.4 p/p_0 in a water adsorption measurement [48]. Considering that we only brought our SURMOFs in contact with water for approximately an hour, structural degradation is most probably not a major concern.

3 Experimental

3.1 Gold nanoparticle synthesis

3.1.1 Materials

Hydrogen tetrachloroaurate(III) anhydrous (≥51% Au, Fisher Scientific), sodium citrate tribasic dihydrate (ACS reagent, ≥99.0% Sigma Aldrich) were used as received. The hydrogen tetrachloroaurate was stored in the fridge at 5 °C, and stored under argon after use. Ultrapure Millipore water (mQ, 18.2 MΩ at 25 °C) was used unless stated otherwise. A 250 mL round bottom flask dedicated to gold nanoparticle synthesis was used, this flask was cleaned before each synthesis with aqua regia (3:1 concentrated HCl:HNO_3) for at least 30min. After treatment with aqua regia the flask was rinsed subsequently with mQ water, ethanol and acetone. Next the flask was placed in an oven at 70 °C to dry. A reflux cooler also dedicated to nanoparticle synthesis was used which was cleaned with water, ethanol and acetone after which it was dried at 70 °C for 30 minutes.

3.1.2 Synthesis

Gold nanoparticles were synthesized using the standard chloroauric acid reduction method which was pioneered by Turkevich [32] and refined by Frens [30]. 10.0 mg $HAuCl_4$ was weighed in a new glass vial using the end of a Pasteur pipette. The $HAuCl_4$ was then quantitatively transferred to the roundbottom flask using 100 mL water. The mixture was then heated up until it started to reflux. When this temperature was reached 700 µL of 1 %(w/w) of a sodium citrate tribasic solution was injected using a finnpipette. The citrate was ejected right into the boiling solution in one fluid motion, so that it did not touch the flask wall. The solution was left to boil for 40 minutes after which a purple-red dispersion had formed which was stored in vials. These vials were kept in the fridge at 5 °C in the dark. Using 700 µL sodium citrate should result in 55 nm gold nanoparticles. Before measuring SERS, the gold nanoparticles were washed 1 time with approximately 5 mL mQ water at 4300 g, to remove remaining reactants. More washing steps would result in particle aggregation because of destabilization of the colloidal solution.

3.2 Silica coated gold nanoparticle synthesis

3.2.1 Materials

(3-aminopropyl)-trimethoxysilane (≥97%, Sigma Aldrich), sodium silicate solution (purum ≥10% NaOH basis, ≥27% SiO_2 basis, Sigma Aldrich), hydrochloric acid (37% fuming, Merck) were used as received. All solutions were prepared using Millipore water. The heating step was performed with a heating plate with a Radley StarFish heating block suitable for three 20 mL vials.

3.2.2 Synthesis

Gold nanoparticles prepared as described in section 3.1.2 were coated with a silica layer according to a slightly modified procedure from Nature Protocols [37]. 1 mL of sodium silicate solution was diluted to 0.54% SiO_2 by adding 1 mL of sodium silicate solution to a 50 mL volumetric flask. Consequently, approximately 20 mL water was added to the flask and 5 mL of 0.06 M HCl. The flask was then filled up to the 50 mL mark with water. The pH of this 0.54% SiO_2 solution was checked with pH paper to make sure it was around 10 which is the ideal pH for SiO_2 shell growth.

15 mL of the 55 nm gold nanoparticle dispersion was transferred to a 20 mL vial. 0.2 mL of 1 mM APTMS was added dropwise while being magnetically stirred at 400 rpm. The mixture was left stirring for 15 minutes to allow the ligand exchange from citrate to APTMS to take place. Next 1.6 mL of the 0.54% SiO_2 was added and the solution was stirred for 3 more minutes. The solution was then heated to 90 °C using a thermocouple (this took about 8 minutes). When it reached this temperature it was kept at 90 °C for 20 minutes, after which it was cooled down in a water bath to room temperature. Finally the SHINs were washed 3 times with mQ water at 4300 g for 10 minutes to remove the reactants thus terminating shell growth. The SHIN samples were stored in the fridge at 5 °C in the dark. The particles were used for measuring SERS within 2 weeks.

3.3 Silver nanoparticle synthesis

3.3.1 Materials

Sodium citrate tribasic dihydrate (ACS reagent, ≥99.0% Sigma Aldrich) and Silver nitrate (ACS reagent, ≥99.0%, Sigma Aldrich) were used as recieved. mQ water was used unless stated otherwise. A 250 mL round bottom flask dedicated to silver nanoparticle synthesis was used, this flask was cleaned before each synthesis with aqua regia (3:1 concentrated HCl:HNO_3) for at least 30min. After treatment with aqua regia the flask was rinsed subsequently with mQ water, ethanol and acetone. Next the flask was placed in a oven at 70 °C to dry. A reflux cooler also dedicated to nanoparticle synthesis was used which was cleaned with water, ethanol and acetone after which it was dried at 70 °C.

3.3.2 Synthesis

Silver nanoparticles were synthesized using the citrate reduction method [34]. 18 mg of silver nitrate was weighed and quantitatively transferred to a 250 mL round bottom flask using 100 mL water. The mixture was refluxed. Next 2 mL of a 1% sodium citrate solution was added. The mixture was kept boiling for another 40 minutes. A milky white solution with a slight shade of yellow-green was obtained. The particles were used the next day for SERS measurements, since silver nanoparticles oxidize quickly.

3.4 synthesis of bulk $Cu(ndc)(dabco)_{0.5}$

3.4.1 Materials

1,4-Diazobicyclo[2.2.2]-octane (98%, Alfa Aesar), Naphtalene-1,4-dicarboylic acid (98%, ABCR GmbH & CO. KG), Copper(II) acetate (98% trace metal basis Sigma Aldrich, Ethanol (absolute, 99.5%, extra dry, Acros organics) were used as recieved.

3.4.2 Synthesis

Bulk $Cu(ndc)(dabco)_{0.5}$ was synthesized by adding 0.670g $Cu(OAc)_2$, 0.187g dabco and 0.728g ndc to 24ml of a 1:1 absolute ethanol-water mixture. The mixture was stirred in a beaker covered with parafilm for 30 minutes. After stirring the mixture was transferred to a teflon coated stainless steel autoclave. The autoclave was placed in a preheated oven at 110 °C for 24h. After heating the autoclave was cooled down in air while still being closed. The contents were then filtrated using vacuum filtration. The residue was washed thrice with absolute ethanol.

3.5 Layer by layer growth of Cu(ndc)(dabco)$_{0.5}$

3.5.1 Materials and instruments

16-Mercaptohexadecanoic acid (99%, Sigma Aldrich), 1,4-Diazobicyclo[2.2.2]-octane (98%, Alfa Aesar), Naphtalene-1,4-dicarboylic acid (98%, ABCR GmbH & CO. KG), Copper(II) acetate (98% trace metal basis Sigma Aldrich, Ethanol (absolute, 99.5%, extra dry, Acros organics) and acetic acid (99.8% for analysis, Acros organics) were used as received. All solutions were prepared using absolute ethanol unless stated otherwise. Gold coated substrates with 60 nm gold and an adhesion layer of germanium on Si (100) wafers were obtained from the nanocenter of Amolf, FOM institute Amsterdam. The substrates were 1 x 1 cm.

Two Ismatec® Reglo-ICC pumps were used to perform the layer by layer synthesis of the SURMOFs. Home written scripts were used for the Ismatec pump software to perform the layer by layer assembly with the right amount of cycles. A double walled reaction vessel was used to maintain a constant temperature. One of the pumps was used to flow either the copper acetate, ndc or dabco solutions into the vessel. The other pump was used to flow absolute ethanol into the vessel and to pump the waste solutions out of the vessel. A Bioforce® UV-ozone cleaner was used to clean the gold substrates.

3.5.2 Synthesis of Cu(ndc)(dabco)$_{0.5}$ SURMOFs

SURMOFs were grown according to the procedure from Zacher et al. [6]. First gold substrates were cleaned with Millipore water, ethanol and acetone. The substrates were then placed in an UV ozone cleaner for approximately 20 minutes to remove any residual organic contaminants. The cleaned gold substrates were then placed in a vial with a few milliliters of 20 mM MHDA in 95% ethanol and 5 % acetic acid to form a MHDA SAM. The substrates were immersed for 24 hours and washed with a solution of 10% acetic acid in ethanol. Next the substrates were placed inside the double walled vessel which was heated at 40 °C. The MOF components were added as solutions in ethanol. 2 mM copper(II) acetate was first added after which 0.2 mM ndc was added and finally 0.2 mM dabco was added. Between each addition of reactants the substrate was immersed in pure ethanol in order to clean it. Table 2 shows the routine required to perform one cylce of MOF growth.

Table 2: Pump operations required to perform one cylce of Cu(ndc)(dabco)$_{0.5}$ surMOF growth.

Time	Pump operation
0	1.5 mL $Cu(OAc)_2$
5'20"	3 mL out
6'00"	1.5 mL EtOH
11'20"	3 mL out
12'00"	1.5 mL NDC
22'20"	3 mL out
23'00"	1.5 mL EtOH
28'20"	3 mL out
29'00"	1.5 mL DABCO
39'20"	3 mL out
40'00"	1.5 mL EtOH
45'20"	3 mL out

4 Results and discussion

4.1 Characterization

4.1.1 UV-visible spectroscopy of gold nanoparticles

UV-vis spectra were measured using a Cary 50 UV-vis spectrometer. Typically 500 µL of the nanoparticles suspension was added to a quartz cuvette together with mQ water. As a background a quartz cuvette containing only mQ water was used. A UV-vis spectrum of a gold nanoparticle suspension is shown in figure 14.

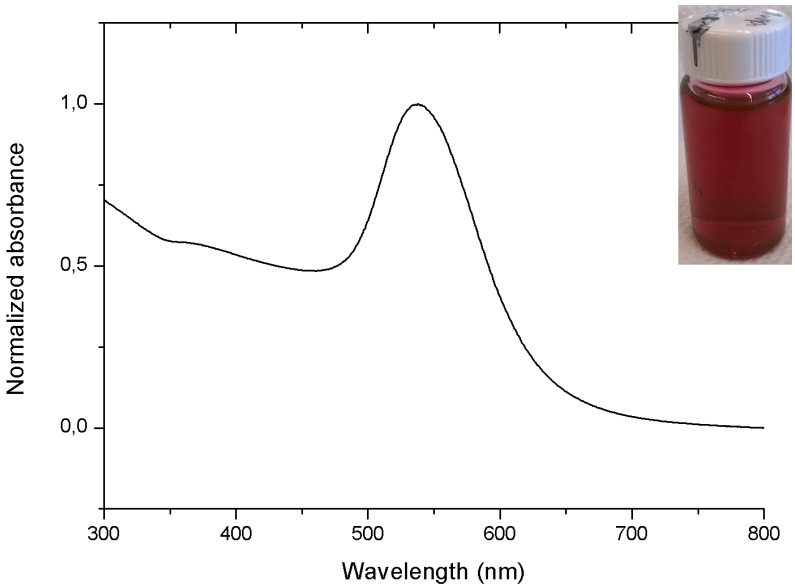

Figure 14: UV-vis spectrum of gold nanoparticles, the absorbance maximum is at 537 nm. The inset shows an image of a vial containing the particles as synthesized.

First of al, a plasmon band is observed, which means that gold nanoparticles were successfully synthesized. Since the position of the plasmon band depends on the size of the gold nanoparticles [49], a rough estimation of the size can be made. From ref [49] we can conclude that the average particle size is around 55 nm. Additionally, we can conclude that the sample is weakly polydisperse, as a very broad plasmon band would be observed for a broad size distribution or multiple particle populations.

4.1.2 Transmission electron microscopy of gold nanoparticles

Transmission electron microscopy images of the gold nanoparticles were taken with a Tecnai 20 FEG electron microscope. In figure 15 TEM images of the gold nanoparticles are shown.

As can be seen in the TEM images gold nanoparticles were succesfully synthesized. The particles are not perfectly spherical but this is expected with an unseeded growth procedure [33]. Furthermore the gold nanoparticles do not have to be perfectly spherical as long as they are SERS active. Using iTEM software the size of about 100 different particles was measured to analyze the particle population. The particles which were analyzed were chosen as randomly as possible. A histogram was made which is shown in figure 16. From the histogram we can conclude that the polydispersity of the synthesized nanoparticles was rather low.

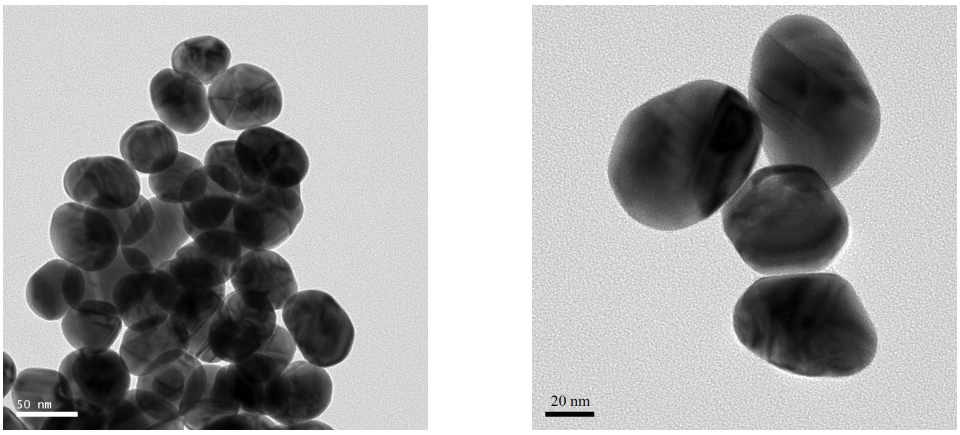

(a) **(b)**

Figure 15: TEM images of gold nanoparticles, weakly monodisperse particles were obtained.

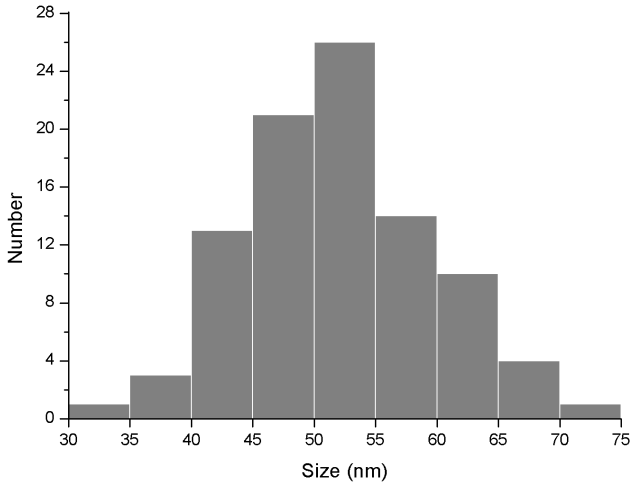

Figure 16: Histogram of the gold nanoparticles as analyzed with iTEM software, the average particle size was 52 nm.

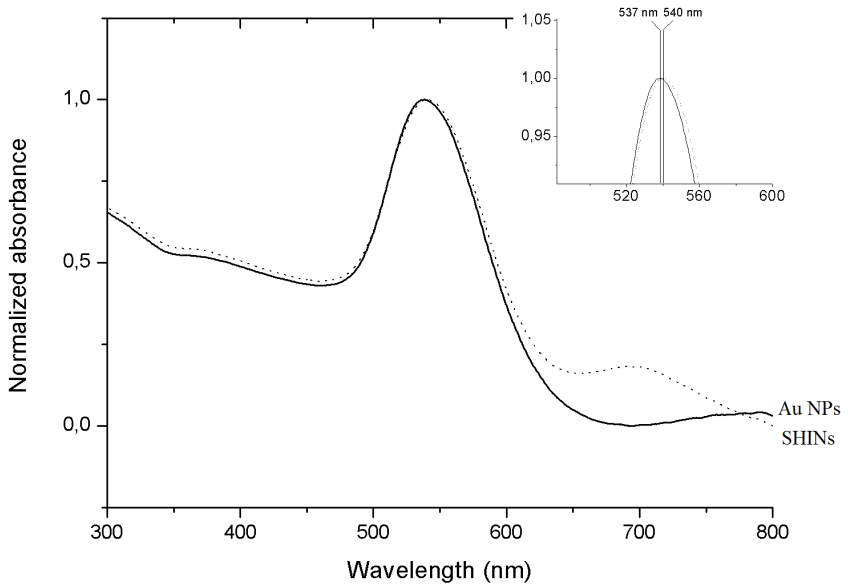

Figure 17: UV-vis spectrum of SHINs compared to the original gold nanoparticles. The absorbance maximum has shifted to higher wavelengths as shown in the inset.

4.1.3 UV-visible spectroscopy of SHINs

To study the effect of the addition of a silica shell to the gold nanoparticles UV-vis spectra of the SHINs were recorded and compared with the original gold nanoparticle spectra. The UV-vis spectra of the original gold particles and the silica coated gold particles are shown in figure 17. As can be seen in the figure the plasmon band has slightly red shifted. This is in agreement with literature, and has been attributed to the change in refractive index of the material surrounding the gold nanoparticle [50]. Furthermore a second smaller band is observed at 715 nm. This band is attributed to the dipolar plasmon resonance which is enhanced by the addition of a silica shell [50]. Consequently, from the spectral red shift we can conclude that most likely a silica shell has been grown around the gold nanoparticles, although not much can be said about the thickness and morphology of the shell.

4.1.4 Transmission electron microscopy of SHINs

To observe the silica shell grown around the gold nanoparticle TEM images of the SHINs were taken. Because of the low contrast of silica compared to gold it is possible to distinguish between the silica shell and the gold core, on the other hand the low contrast makes observing the silica shell rather difficult against the TEM grid film. In figure 18 the TEM images are shown.

As can be seen in the images a silica shell was succesfully synthesized around the particle. We did not find any particles with missing or incomplete silica shells. Different from the gold nanoparticles these particles did not aggregate upon drying, leading to evenly spaced particles over the TEM grid. This made it in view of time impossible to do a size analysis because we would have to make hundreds of images to make the results statistically relevant. However, from literature it seems that the gold core barely changes when the particles are coated with silica, so we can assume that the gold core still has an average size of 52 nm [37]. Making the average particle size of the SHINs 56 nm. The different drying effect on the TEM grid is also an indication that the particle-particle interaction has changed upon coating. This can be beneficial when applying the particles to the SURMOF, because, if the particles

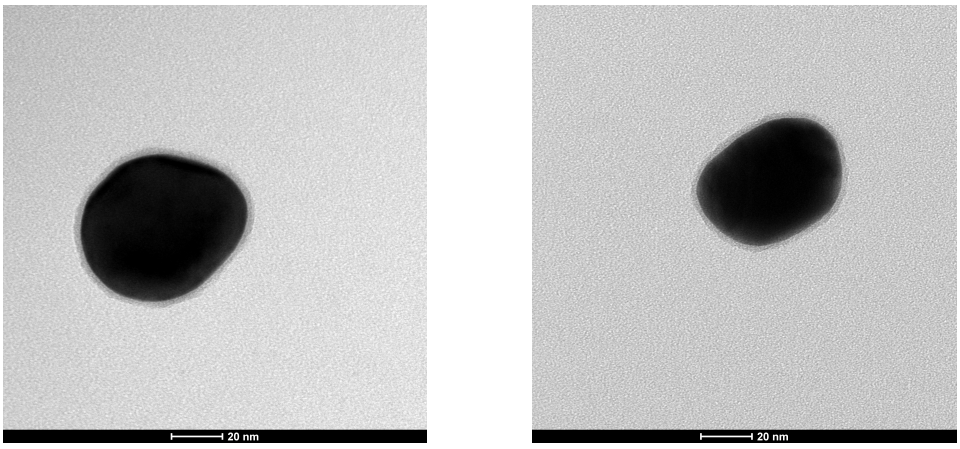

(a) **(b)**

Figure 18: TEM images of SHINs, a silica shell can clearly be seen. The average shell thickness was 2.5 nm as measured with iTEM. No aggregated particles were found and no detached silica was found. In appendix A an EDX spectrum of the sample is shown.

do not aggregate as easily they might spread more homogeneously over the SURMOF.

4.1.5 Pinhole testing of SHINs

To test whether the silica shells were pinhole free, a pinhole test was performed as described in ref [37]. 10 µL of the particle dispersion was deposited on a silicon wafer using a Finn pipette. The droplet was left to dry. Next 10 µL of 10 mM pyridine was added. A glass coverslip was directly added to minimize evaporation of the water and pyridine. Raman measurements were performed on this sample to check for the presence of pyridine chemisorbed onto gold. This is used as an indication for pinholes. In figure 19 the results of the pinhole test are shown.

As can be seen in the figure no pyridine band is observed on the SHIN sample. Therefor we can conclude that the silica shell, which was already observed with TEM, is indeed free of any pinholes. This makes the particles suitable for our experiments.

4.1.6 UV-visible spectroscopy of silver nanoparticles

UV-vis spectra of the silver nanoparticles were measured. One of the spectra can be seen in figure 20. Similar to the gold nanoparticles, a plasmon band is observed, indicating the formation of nanosized silver. Because the suspension absorbs blue light it appears yellow when looking through the vial at a light source. The silver suspension is also much more turbid than the gold suspension. This is probably due to the higher concentration of metal precursor used in the synthesis, resulting in bigger or more particles.

When looking at the UV-vis spectrum of silver we can see that not only the position of the plasmon band is different from gold, but also the shape. The band appears to have a small shoulder at 365 nm. Furthermore, it has a tail on the right side. These features can again be explained in terms of dipolar and quadrupolar plasmon resonance [22]. The small shoulder at 365 nm is probably due to the quadrupolar plasmon resonance of the smallest particles in the sample, having the highest energy. The big tail is probably an ensemble of dipolar plasmon bands of the biggest fraction silver nanoparticles, as the prominence of the lower energy dipolar plasmon band increases with size [22]. So from UV-vis we can conclude that silver nanoparticles have succesfully been synthesized. Most likely the particles are

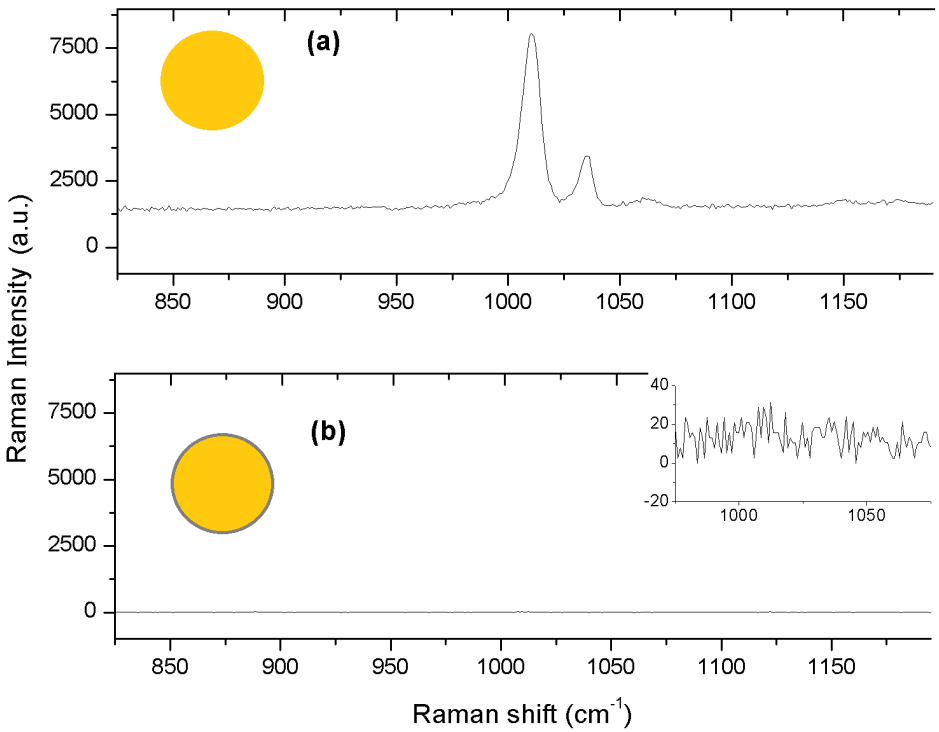

Figure 19: Pinhole testing of the SHINs (a) shows the test performed on bare gold nanoparticles showing adsorbed pyridine bands at 1010 cm^{-1} and 1035 cm^{-1}. (b) shows the test performed on the SHINs, no bands are observed in this case. The inset shows that only noise is measured where the pyridine band would be. Measurements were done using 50x objective, 1 second exposure time, 785 nm at 0.05% intensity and a 1200 l/mm grating.

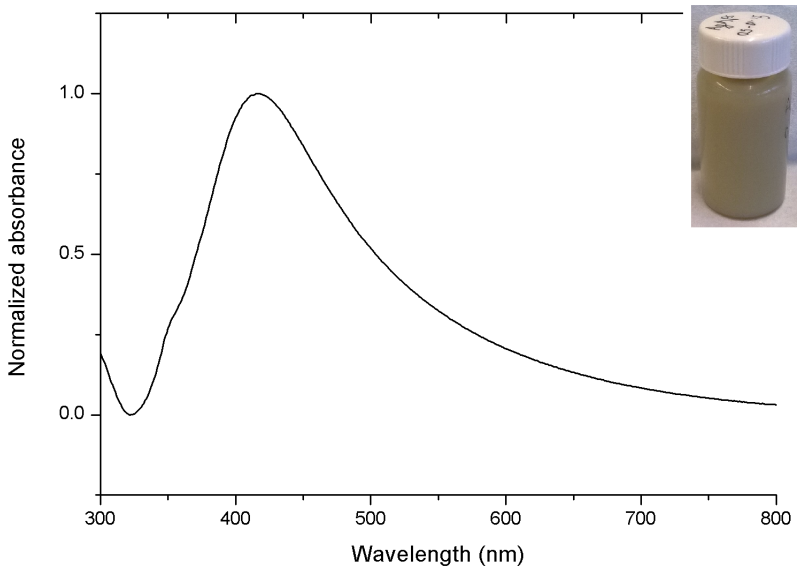

Figure 20: UV-vis spectrum of the silver nanoparticles, the absorbance maximum is at 417 nm. The inset shows an image of a vial containing the silver nanoparticles.

bigger because they scatter light more strongly. Also we expect a bigger spread in particle size as indicated by shape of the plasmon band.

4.1.7 Transmission electron microscopy of silver nanoparticles

TEM images of the silver nanoparticles were made using a Tecnai 20 FEG electron microscope. In figure 21 some images of the silver nanoparticles are shown. As can be seen, particles were succesfully synthesized. The silver nanoparticles are less uniform and monodisperse than the gold nanoparticles, this is expected as silver is easily oxidized in early growth stages leading to non spherical particles. However, as long as the particles are SERS active they can be used. A histogram of the silver nanoparticle population is shown in figure 22.

4.1.8 AFM images of the substrates

AFM images of the SURMOF substrates were made using a NT-MDT® NTEGRA Spectra atomic force microscope. HA_NC Etalon probes were used which were operated at a frequency of 220 kHz ±10%. The probes have a force constant of 7.2 N m^{-1} ±20 % and the radius of curvature was 10 nm. AFM scans of the samples 2, 5, 10 and 20 cycles were made.

In figure 23 the AFM scans of the 2 cycle sample are depicted. Little islands of SURMOF with typical lateral dimensions of 200 nm are observed. The heigth of the islands is about 20-40 nm. A rather corrugated surface is created this way especially after more deposition cycles. The existance of islands implies that the SURMOF does not grow in a perfect layer by layer fashion, but rather in a nucleation-growth like mechanism. It appears that making the first small crystal of MOF is unfavorable, but once a nucleus has formed the growth proceeds more easily. This observation is in agreement with literature [8].

In figure 24 the AFM scans of the 5 cycles sample are depicted. As can be seen in the figure more SURMOF islands appear per unit area compared to the 2 cycle sample. The islands have also grown bigger, around 350 nm. However, there is still a lot of open stubstrate in between the SURMOF. This means that in the SERS experiments still manyf nanoparticles are touching the gold substrate.

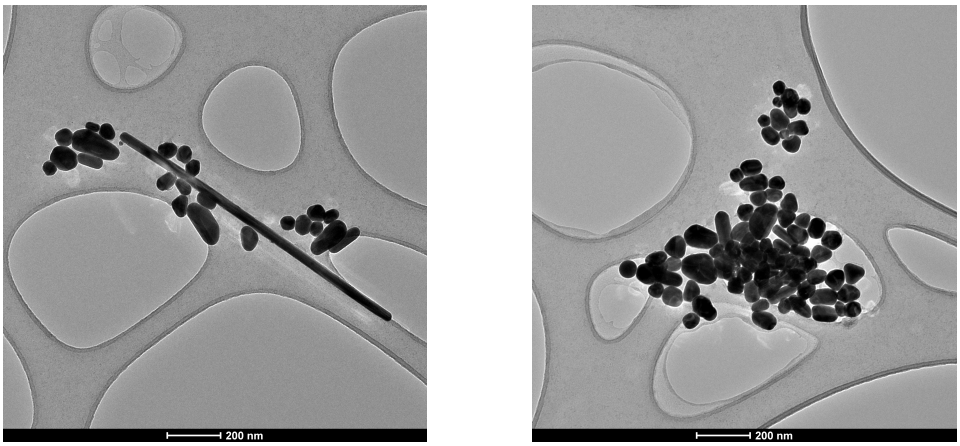

(a) **(b)**

Figure 21: TEM images of the silver nanoparticles. As can be seen the particles are less monodisperse than the gold nanoparticles. Also elongated rod like structures were observed.

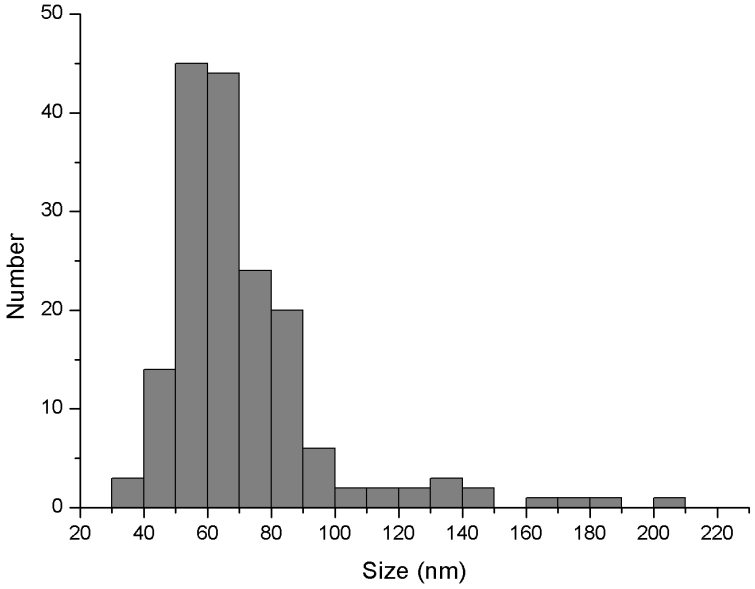

Figure 22: Histogram of the silver nanoparticles as analyzed with iTEM software, the average particle size was 74 nm. The elongated rod like structures were excluded from this measurement. 170 particles were measured. As can be seen the spread in particle size is much bigger for silver than for gold.

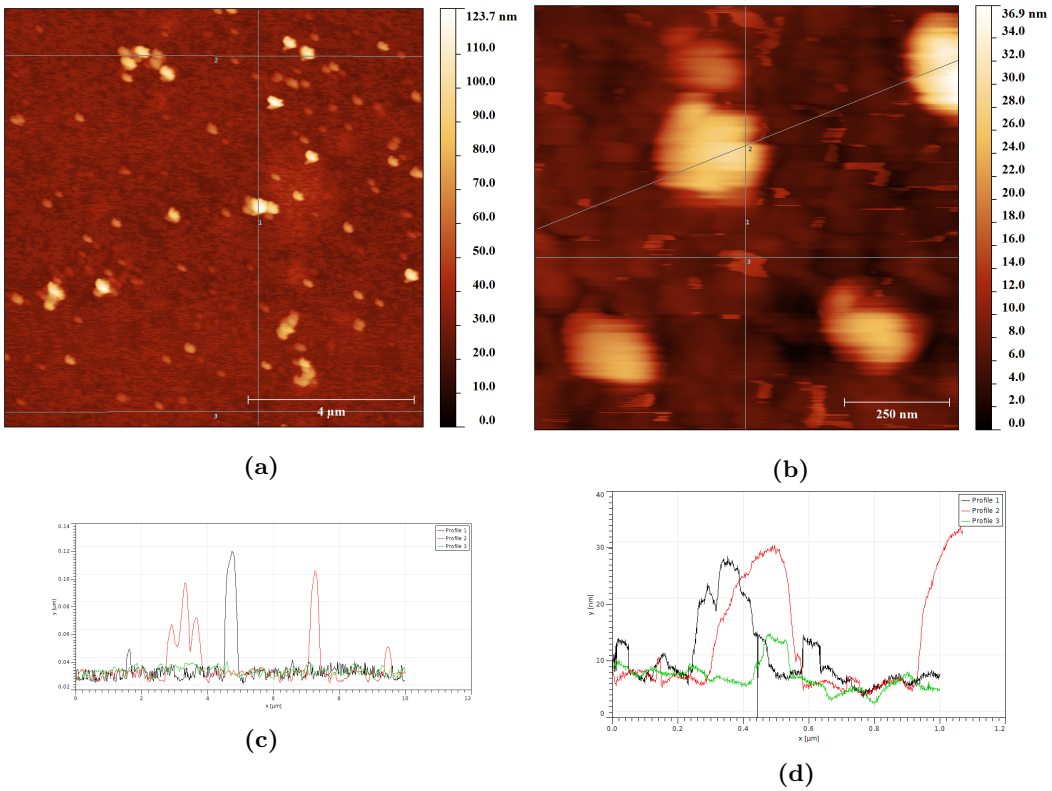

Figure 23: AFM images of the 1 deposition cycle sample. (a) and (b) show AFM scane with different magnification. (c) and (d) show the height profiles at the positions as indicated in the AFM scans with lines.

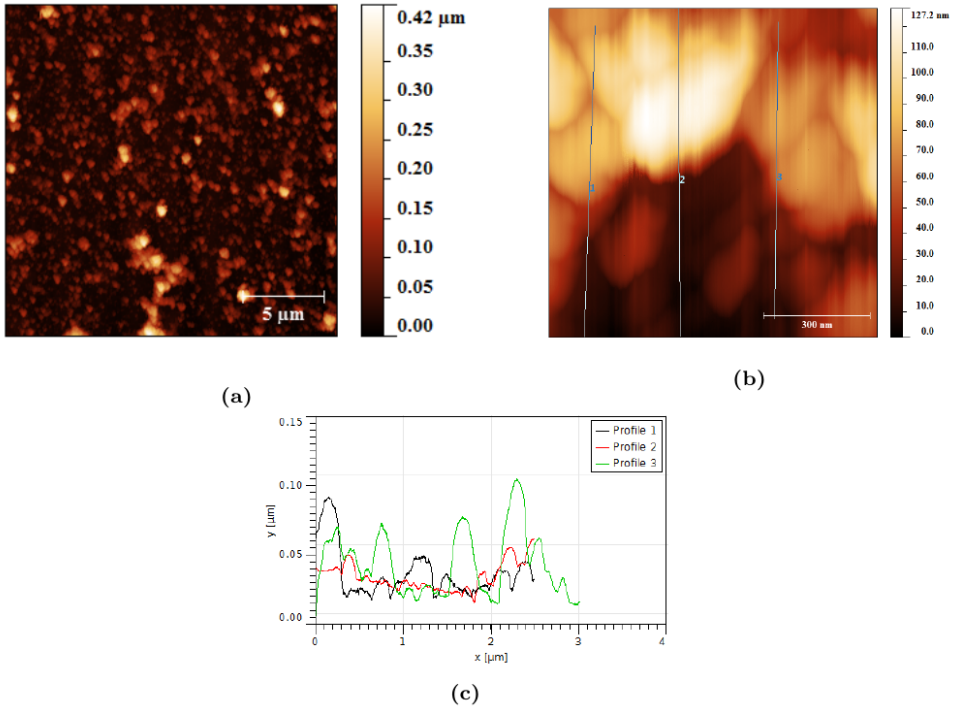

Figure 24: AFM images of the 5 deposition cycles sample. (a) and (b) show AFM scans with different magnification. (c) shows the height profiles of the lines indicated in (b).

In figure 25 the AFM scans of the 10 cycle sample are depicted. In these images it can be seen that the MOF island have grown even larger, to a size of about 600 nm. The height of these islands has increased to around 400 nm. There is some open substrate but most of the substrate seems to be covered with at least some MOF.

In figure 26 an AFM scan of the 20 cycle sample is shown. As can be seen in the figure, most of the islands are grown together to form a layer almost covering the entire substrate. This could be the reason that there is a drop in SERS signal in the measurements when we get to the 20 cycle sample. Because the SERS active particles are so far away from the gold substrate that a possible plasmon coupling between the planar gold substrate and the gold or silver nanoparticle becomes unlikely. Furthermore, it could very well be that because of this strongly crumpled surface the SERS signal is stronger. In case we had an atomically flat layer of MOF there would be less MOF in between the enhancing particles because there are no protuberances sticking out of the surface. Because the electric field effect is especially strong in between the nanoparticles, a very flat surface would most likely give less signal (apart from the reason that the amount of surface is smaller).

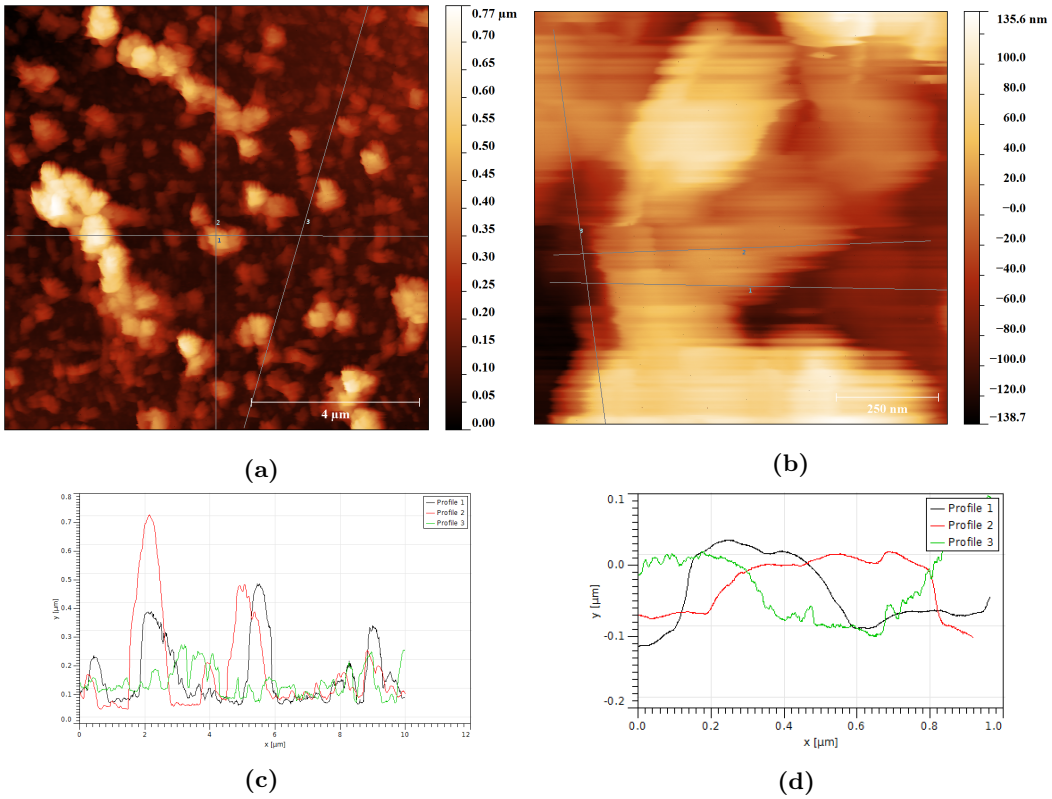

Figure 25: AFM images of the 10 deposition cycles sample. (a) and (b) show AFM scane with different magnification. (c) and (d) show the height profiles at the positions as indicated in the AFM scans with lines.

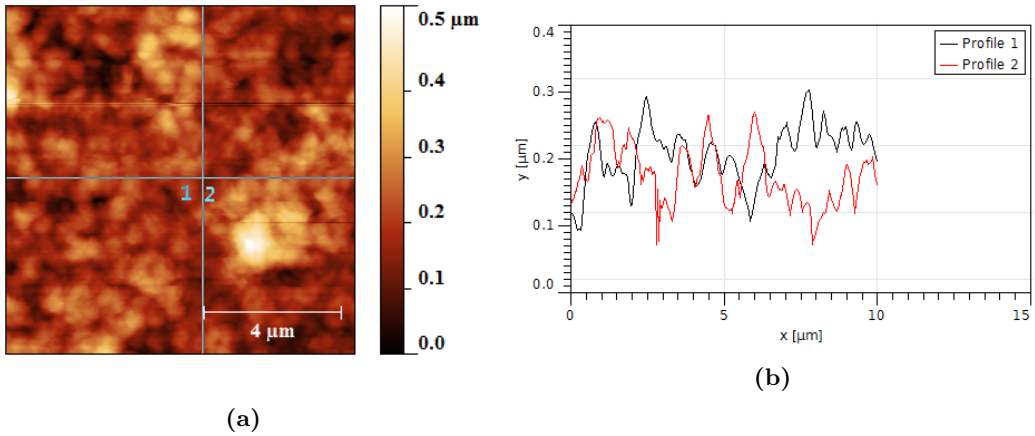

Figure 26: AFM image of the 20 deposition cycles sample. (a) shows AFM the AFM scane (b) shows the height profiles at the positions as indicated in the AFM scan with lines. It is clear that in this sample almost the entire substrate is covered with MOF.

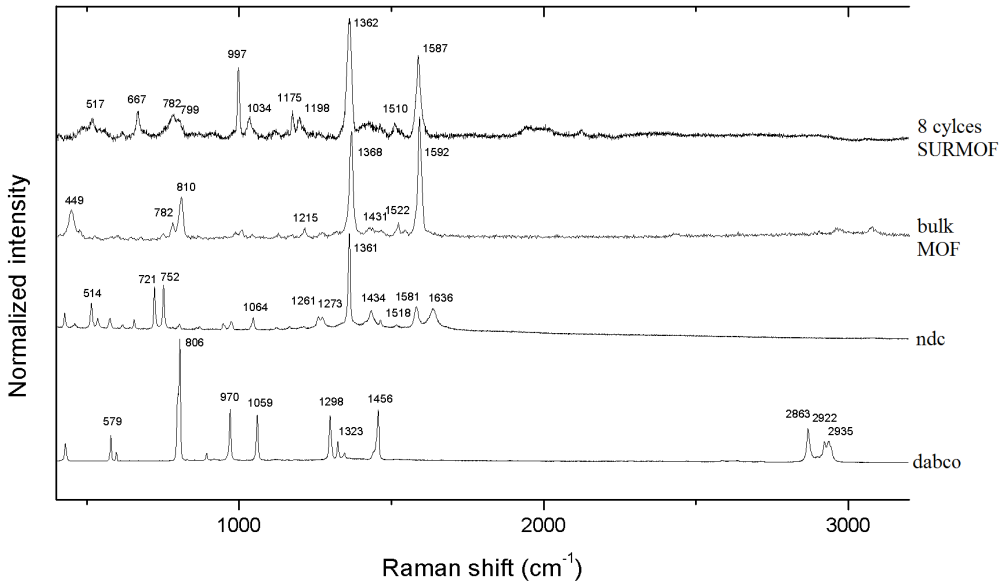

Figure 27: Raman spectra of ndc, dabco and bulk Cu(ndc)(dabco)$_{0.5}$. Measured with 50x objective, 532 nm at 0.05% laser intensity. A SERS measurement of 8 cycles Cu(ndc)(dabco)$_{0.5}$ SURMOF is also included.

4.2 Raman measurements

For Raman spectra measurements a Renishaw InVia spectrometer coupled to a Leica DM LM microscope with a computer controlled XY stage was used. As light sources a 500 mW 532 nm frequency doubled Nd:YAG laser was used, and a 500 mW 785 nm diode laser. A leica 50x N_plan objective with 0.75 numerical aperture was used. For each measurement the laser intensity, the exposure time, the amount of accumulations and the grating used is specified.

4.2.1 Peak assignment of MOF components

Before the SERS measurements of the SURMOFs are shown we make an analysis of bands observed in the components of the MOF: ndc and dabco. A Raman spectrum of copper(II)acetate is not shown in this figure as it only shows a big fluorescence background and no vibrations, the spectrum is included in appendix B . It is not possible to assign all bands, but by assigning the most prominent bands we can more clearly analyze the SURMOF spectra. In figure 27 the Raman spectra of dabco, ndc, bulk Cu(ndc)(dabco)$_{0.5}$ and a Cu(ndc)(dabco)$_{0.5}$ SURMOF 8 cycles SERS measurement is shown.

In the dabco Raman spectrum the bands at 2935, 2922, 2863, 1456, 1298 cm^{-1} all correspond to CH_2 vibrational modes as shown in table 3. The bands at 1059, 806 ad 576 cm^{-1} correspond to NC_3 vibrational modes. Additionally a band at 970 cm^{-1} is observed which is ascribed to a mixed C-C stretch + CH_2 wagging vibration [51]. In the ndc Raman spectrum the bands at 1581, 1518 and 1361 cm^{-1} correspond to naphthalene ring vibrations as shown in table 4 [52]. The bands at 1636, 1433, 1273, 1261 and 721 cm^{-1} correspond to carboxylic acid vibrations [52]. The bands involving the carboxylic acid groups are expected to shift or dissapear completely in the MOF structure, since these groups will become doprotonated and coordinated to the copper ions.

Table 3: Peak assignment of 1,4-diazabicyclo[2.2.2]octane compound, all assignments were taken from [53].

Peak position (cm^{-1})	Assignment
2935	CH_2 assymetric stretch
2922	CH_2 assymetric stretch
2863	CH_2 symetric stretch
1456	CH_2 scissoring
1298	CH_2 twisting
1059	NC_3 assymetric stretch
970	C-C stretch + CH_2 wagging
806	NC_3 stretch
579	NC_3 stretch

Table 4: Peak assignment of1,4 naphthalenedicarboxylate.

Peak position (cm^{-1})	Assignment
1636	C=O stretch [52]
1581	C=C stretch [52]
1518	C=C stretch [52]
1433	C−O stretch + O−H deformation
1361	C=C stretch [54]
1273 and 1261	C−O stretch doublet [52]
752	C−H out of plane [52]
721	O−H deformation [52]

4.2.2 SERS measurements on SURMOF using gold nanoparticles

Gold nanoparticles were drop casted onto the SURMOF by pipetting 10 µL of gold nanoparticles solution on the SURMOFs. The droplet was left to dry and next Raman measurements were done. It was found that the quality of the measured Raman spectra decreased drastically over time, so all spectra were measured within one day of dropcasting the particles.

In figure 28 the results of the surface enhanced Raman measurements are shown. The image only shows the 400 to 2300 cm^{-1} region because all vibrations observed were in this region. Furthermore a very strong band is always observed at 135 and 293 cm^{-1} These two bands were present for every spectrum measured with 785 nm excitation and most likely a d-d transition of the copper(II) species is excited [55], resulting in resonance Raman. Because these bands are so intense compared to the rest of the spectrum, the Raman measurements were performed from 400 to 3200 cm^{-1} to keep the CCD from being damaged, while still getting sufficient signal to observe the other MOF bands.

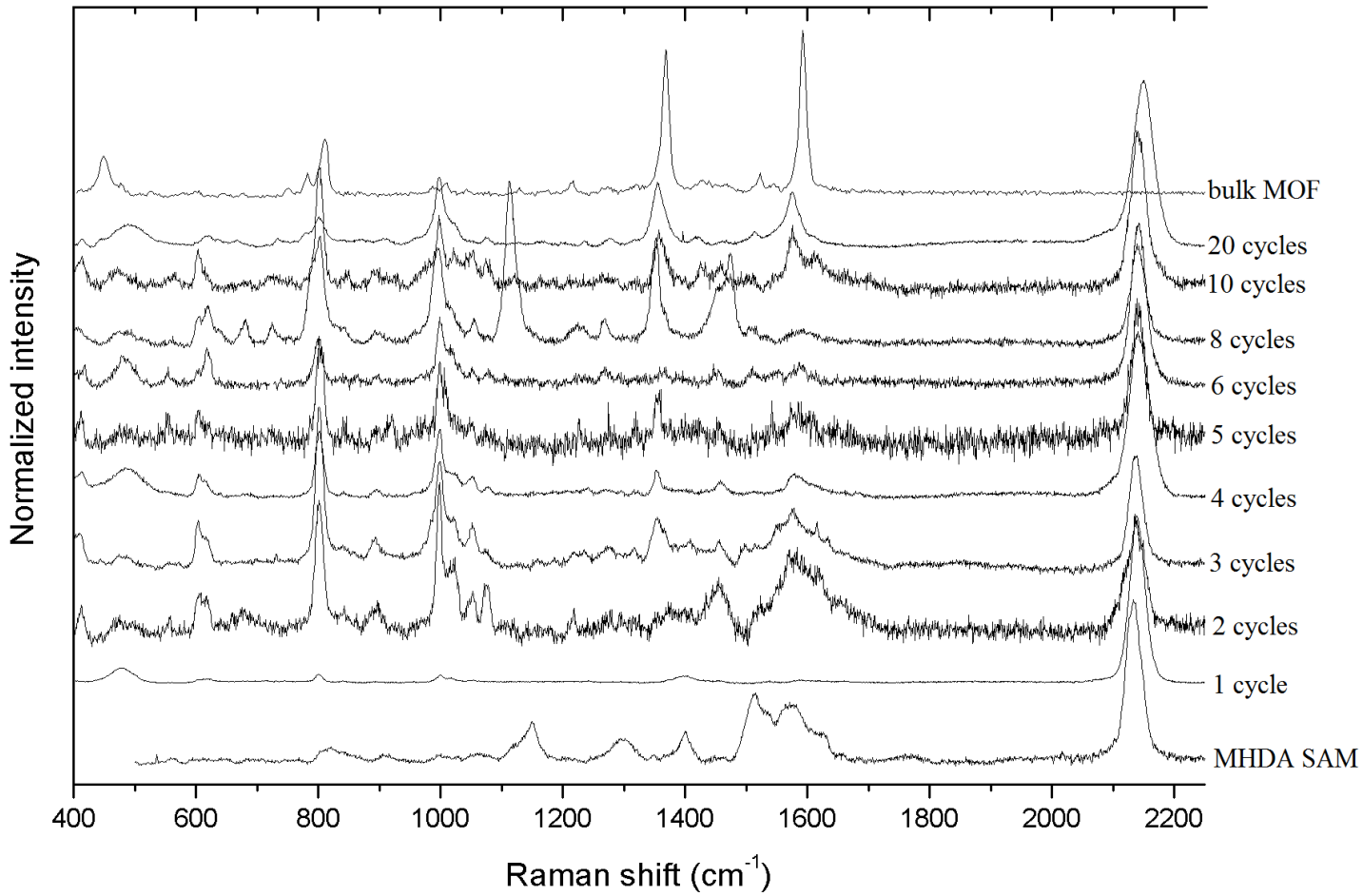

Figure 28: Stacked Raman spectra of all Cu(ndc)(dabco)$_{0.5}$ samples measured with gold nanoparticles. The top spectrum is not a SERS measurement but just a regular Raman measurement of bulk Cu(ndc)(dabco)$_{0.5}$. The SERS measurements were all performed with a 785 nm laser operating at 0.05% laser power. A 50x objective was used with a 1200 l/mm grating. The exposure time was 10 seconds, the amount of accumulations varied from 3 to 5 depending on the quality of the spectrum. A background correction was performed using Renishaw Wire software using the cubic spline setting. The SERS spectra were normalized to the citrate band. In appendix F the original SERS spectra with background are shown. In appendix D optical images of the samples are shown with crosshair indicating were the measurement was performed.

As can be seen in figure 28 each SERS spectrum has a strong band around 2138 cm^{-1}, this band is assigned to either the citrate ions or reaction products like 1,3-dicarboxyacetone adsorbed on the gold nanoparticles [56,57]. Another band which is observed in every SURMOF spectrum is the band at 800 cm^{-1} from the NC_3 group in dabco. This band is relatively more enhanced in the SERS spectrum with respect to the other bands. An explanation could be that the exposed nitrogen atoms adsorb on the gold surface causing chemical enhancement of the Raman signal. This would also explain the slight shift of the band when measured with SERS instead of Raman spectroscopy. Another band which is very prominent in every SERS spectrum is the band at 997 cm^{-1}. This band is assigned to a mixed C-C stretch + CH_2 wagging vibration [51]. The naphthalene ring vibrations at 1362 and 1587 cm^{-1} are sometimes visible in the SERS spectra but not always. A summary of bands observed in the gold SERS spectra and other SERS spectra is given in table 5.

From the gold nanoparticle SERS data we can conclude that we have successfully observed the SURMOF. The ndc and dabco bands are visible even after 1 deposition cycle. The spectra are, however, not very consistent. Especially the ndc bands greatly vary in intensity between different measurements. Concludingly, we can say that gold nanoparticles can be used to measure the SURMOF spectra but the spectral differences between the samples is big.

4.2.3 SERS measurements on SURMOF using SHINs

SHINs were drop casted onto the SURMOF by depositing 10 µL of SHIN solution on the SURMOFs. The droplet was left to dry and next Raman measurements were performed.

In figure 29 the Raman spectra of the SERS experiments using SHINs are shown. The image shows the 400 to 1900 cm^{-1} region which contains all visible bands. In appendix E the entire region from 400 to 3200 cm^{-1} is shown.

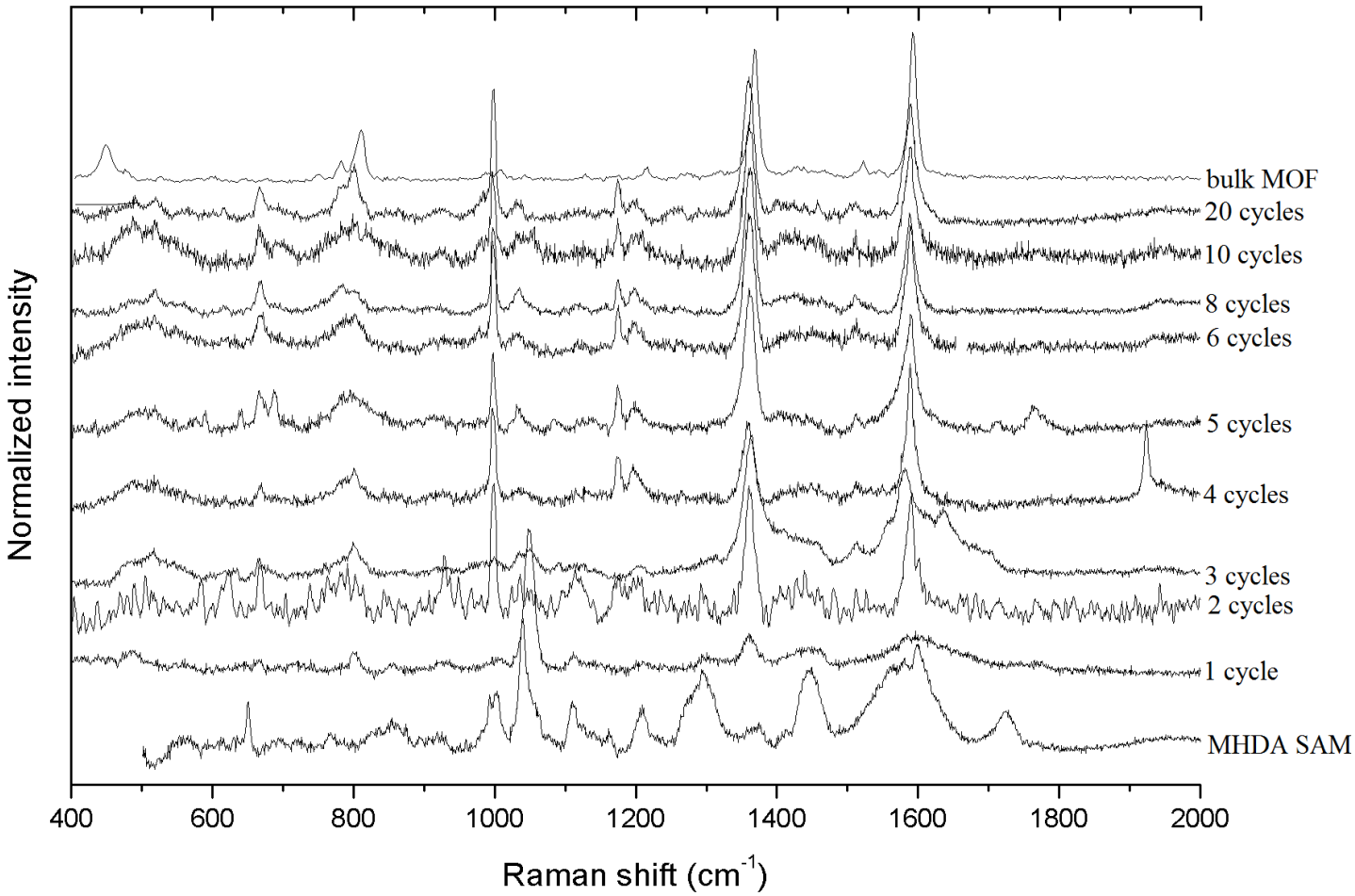

Figure 29: Stacked Raman spectra of all Cu(ndc)(dabco)$_{0.5}$ samples measured with SHINs. The SERS measurements were all performed with a 785 nm laser operating at 0.05% laser power. Except for the 8, 10 an 20 cycles samples which were measured at 0.1% laser power. A 50x objective was used with a 1200 l/mm grating. The exposure time was 10 seconds, the amount of accumulations varied from 1 to 4 depending on the quality of the spectrum. A background correction was performed using Renishaw Wire software using the cubic spline setting. In appendix F the original SERS spectra with background are shown. In appendix D optical images of the samples are shown with crosshair indicating were the measurement was performed. All spectra were normalized to the 1362 cm^{-1} band except for the 1 cycle sample which was normalized to the 1050 cm^{-1},

First of all, the band at 2138 cm^{-1} caused by citrate molecules or reaction products is not visible when using SHINs. This confirms that the ligand exchange from citrate/reaction products to APTMS was successful. It also indicates that no additional molecules are introduced into the system, the SHINs are thoroughly washed so the SURMOFs are only exposed to clean silica. This is also illustrated in appendix C.

The NC_3 band at 800 cm^{-1} is still visible in the SHIN spectra as a broad band. They are however, much less pronounced. This confirms that this vibration probably experiences chemical enhancement in the gold nanoparticle SERS measurement. Interestingly three new bands appears at 667, 1174 and 1199 cm^{-1} which are not visible in the gold nanoparticles SERS spectra. The origin of these bands is unknown. The band at 997 cm^{-1} is still visible just as in the gold nanoparticle SERS spectrum. Furthermore the naphthalene ring vibrations at 1362 and 1587 $cm^{-1}$are visible in every spectrum. Even the one cycle sample shows the 1362 cm^{-1} naphthalene ring vibration. This indicates that even after 1 cycle there is a detectable amount of SURMOF component on the substrate which is remarkable. The 2 and 3 cycles samples already clearly show the Raman spectrum of the SURMOF, although the 3 cycle sample does seem to have some impurities. A summary of bands observed in the SHIN SERS spectra and other SERS spectra is given in table 5.

When all the cycles are compared a general trend can be observed: from 1 to 4 deposition cycles the MOF spectra become more clearly visible. From 4 deposition cycles onwards the spectra look consistent. This confirms the theory that every cycle more MOF is grown on the substrate. From the fourth deposition cycle not much change is seen because the SERS measurement only probes the top layer since the volume of the enhanced field is in the order of nm, hence only the top layer is probed where the particles are situated. To conclude we can say that silica coated gold nanoparticles give more consistent results than the gold nanoparticles.

4.2.4 SERS measurements on SURMOF using silver nanoparticles

Silver nanoparticles were drop casted onto the SURMOF by pipetting 10 µL of silver nanoparticles solution on the SURMOFs. The droplet was left to dry and next Raman measurements were done. It was found that the quality of the measured Raman spectra decreased drastically over time, so all spectra were measured within one day of dropcasting the particles. It was also found that with the 532 laser the sample was much easier burned which means only one accumulation could be used as more accumulation caused to much radiation damage. This also made it much more difficult to make chemical maps with the silver nanoparticles because the sample was already burnt before good spectra could be measured.

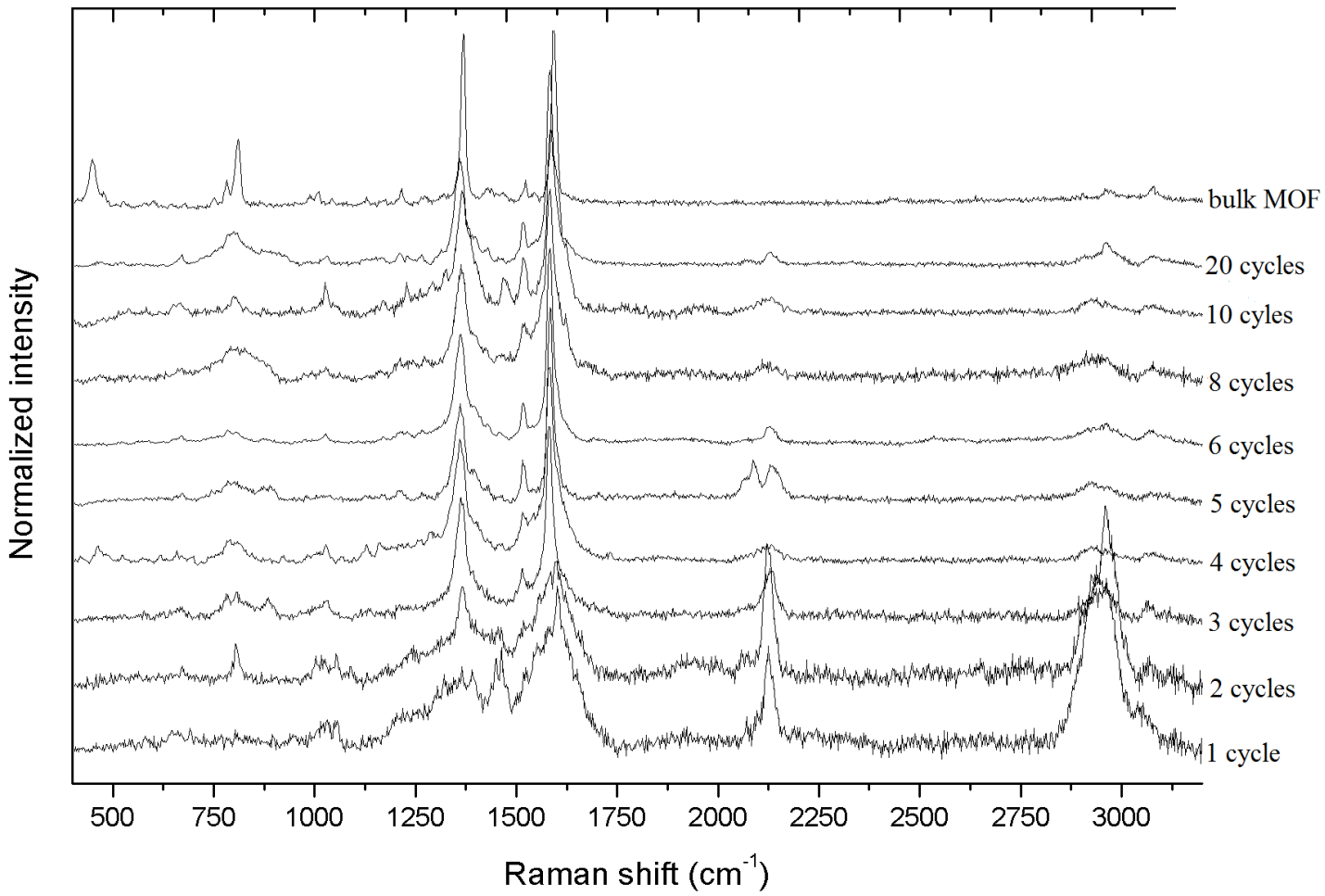

Figure 30: Raman spectra of all Cu(ndc)(dabco)$_{0.5}$ samples measured with silver nanoparticles. The top spectrum is not a SERS measurement but just a regular Raman measurement of bulk Cu(ndc)(dabco)$_{0.5}$. The SERS measurements were all performed with a 532 nm laser operating at 0.05% laser power. A 50x objective was used with a 1200 l/mm grating. The exposure time was 10 seconds and every measurement was just one accumulation. A background correction was performed using Renishaw Wire software using the cubic spline setting. The spectra were normalized to the 1517 cm^{-1} band. In appendix F the original SERS spectra with background are shown. In appendix D optical images of the samples are shown with crosshair indicating were the measurement was performed.

Similar to the gold nanoparticles, a band is visible at 2127 cm^{-1}, which is most likely the citrate ions or reaction products adsorbed on the silver nanoparticles [56,57]. The bands are however less intense than with the gold nanoparticle measurement. Another difference from the gold spectra is the appearance of bands corresponding to CH_2 vibrations at around 2946 cm^{-1} . With 785 nm excitation and gold nanoparticles these bands were not visible. We think that these bands originate from the citrate ligands or other reaction products because it seems that the intensity of these bands is scales the same as the intensity of the band at 2131 cm^{-1}. If we take a look at cycles 1, 2 and 3 we can clearly see that the intensities of these bands are related. So these CH_2 vibration bands are most likely not originating from the dabco molecules. A summary of bands observed in the silver nanoparticle SERS spectra and other SERS spectra is given in table 5.

In the silver nanoparticle SERS spectra only four bands coming from the SURMOF can be identified. The dabco band at 997 cm^{-1} is visible although it is a weak broad band. Furthermore the naphthalene ring vibrations at 1362, 1517 and 1587 cm^{-1} are visible. The most important results is that the bands belonging to the MOF seem to increase in intensity with respect to the citrate bands when going from bottom to top. This indicates that indeed more MOF structure is deposited each cycle.

Table 5: Summary of the bands observed in the different SERS measurements, vibration energies are given in cm^{-1}. Next to the wavenumber the intensity of the band is denoted with (s) for strong, (m)for medium and (w) for weak

Vibration	bulk MOF	gold SERS	AuSHIN SERS	silver SERS	compound	assignment	ref
1	3076(w)			3070(w)	dabco	CH_2 asymmetric stretch	[52]
2	2971(w)			2959(w)	dabco	CH_2 symmetric stretch	[51,53]
3				2946(m)	citrate/reaction products	CH_2 symmetric stretch	[52]
4		2140(s)		2127(m)	citrate/reaction products	C=O stretch	[56]
5	1592(s)	1573(m)	1587(s)	1583(s)	ndc	C=C stretch	[52,54]
6	1522(w)		1512(w)	1518(m)	ndc	C=C stretch	[52,54]
7	1368(s)	1354(m)	1358(s)	1360(s)	ndc	C=C stretch	[52,54]
8	988(w)	995(s)	998(s)		dabco	C-C stretch/CH_2 wagging	[51]
9	810(m)	800(s)	800(w)	804(w)	dabco	NC_3 symmetric stretch	[51]
10	782(w)		782(w)	784(w)	dabco	NC_3 symmetric stretch	[51]

4.2.5 Semi-quantification of the SERS spectra

To further analyze the results the bands in the SERS spectra can be integrated and their intensities can be compared. We should mention that real quantification of the results is impossible as the SURMOF band intensities do not only depend on the thickness of the SURMOF but also on the amount of enhancing nanoparticles that are located on top. By dropcasting the nanoparticles, drying effects cause the particles to be deposited in a ring-like fashion, similar to a coffee stain. This means that the particles are not distributed homogeneously. This is the reason why real quantification of the results is not possible.

In the gold nanoparticle SERS spectra we can use the citrate band as an internal standard to normalize the dabco and ndc bands to. The citrate band area is a measure for the amount of gold nanoparticles enhancing the Raman signal. This is not very rigorous as some of the gold nanoparticles may not even touch the SURMOF: this depends on the thickness of the nanoparticle layer deposited on top. However, on average we hope to see an increase in area of the ndc and dabco bands with respect to the citrate band, since the amount of SURMOF should increase. In figure 31 the integration data are shown. In the figure we see a positive slope. This is an indication that the SURMOF layer grows each cycle.

In the SHIN SERS spectra there are no citrate bands to use as internal standard. We can however, compare the dabco and ndc band intensity. This gives us information about the structural integrity of the SURMOF under experimental conditions, since the intensity of the dabco and ndc bands should be correlated in a linked MOF structure. In figure 32 the ratio of dabco and ndc band area are plotted for the gold nanoparticle and SHIN SERS measurements. As can be seen in the figure the ratio dabco/ndc is higher for the gold nanoparticles measurement, this is evidence for a chemical enhancement effect taking place when gold nanoparticles are used. The dabco molecules might adsorb on the gold nanoparticles, this is unwanted since we want to measure the SURMOF Raman spectrum without changing the system. Furthermore the ratio dabco/ndc is much more consistent when SHINs are used. This might indicate that the structure of the SURMOF is conserved better when SHINs are used in stead of gold nanoparticles. Consequently, the SHINs seem to interfere less with the system than the gold nanoparticles.

Not all Raman spectra were measured using the same laser intensity, although the measurements in which equal laser power was used can be compared. For the SHIN spectra these were the spectra with 2, 4, 6, 8, 10 and 20 immersion cycles respectively. In figure 33 the plot is shown. As can be seen the amount of SURMOF does increase with the number of immersion cycles only the sample with 20 immersion cycles deviates strongly from this trend. All silver spectra were measured with the same laser power meaning they can all be compared. In figure 34 the ndc band intensity is plotted against the amount of immersion cycles. As can be seen in the figure, an increase in amount of ndc is observed. Indicating that the SURMOF has grown.

4.2.6 Raman maps of the SURMOFs

Raman maps of the naphthalene C=C stretch vibration at 1362 cm^{-1} were made using SHINS as signal enhancer. Only SHINs were suitable for making Raman maps, as the gold nanoparticles seemed to destroy the SURMOFs and the 532 nm laser needed to measure with silver nanoparticles caused to much radiation damage when measuring maps, due to the long exposer time needed.

At low laser intensity this C=C stretch was the most intense band in the Raman spectra, also the C=C stretch vibration at 1597 was visible it was however less intense. The chemical maps were constructed by performing a streamline images acquisition over the sample using 5% laser power. It was found that the bands were only visible if particles were located on top of the SURMOF. Chemical maps of every sample were measured. However, only samples 1,

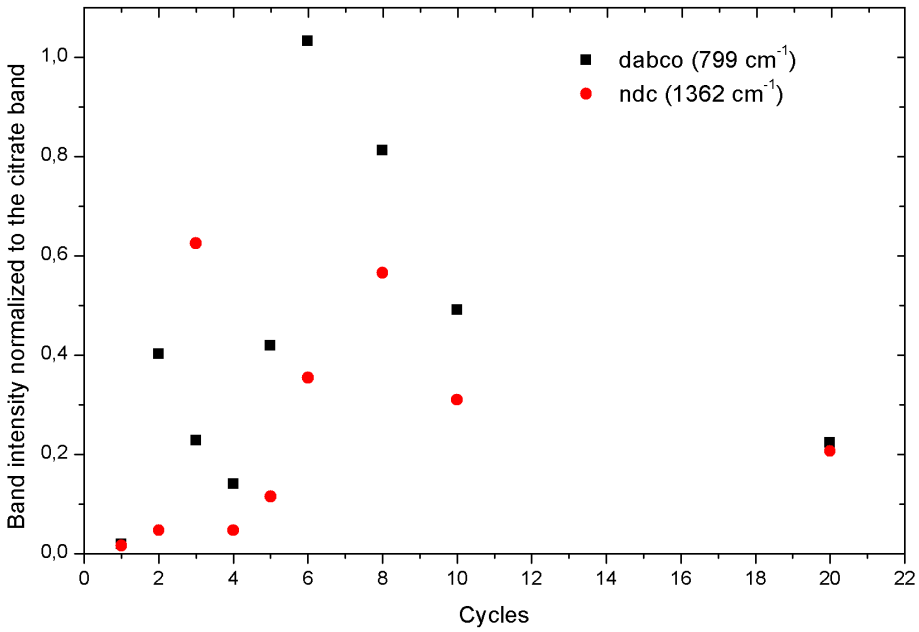

Figure 31: Band integration of the gold SERS measurement. The area of the 799 cm^{-1} dabco and the 1362 cm^{-1} ndc band are divided by the area of the 2140 cm^{-1} citrate band and plotted against the amount of cycles.

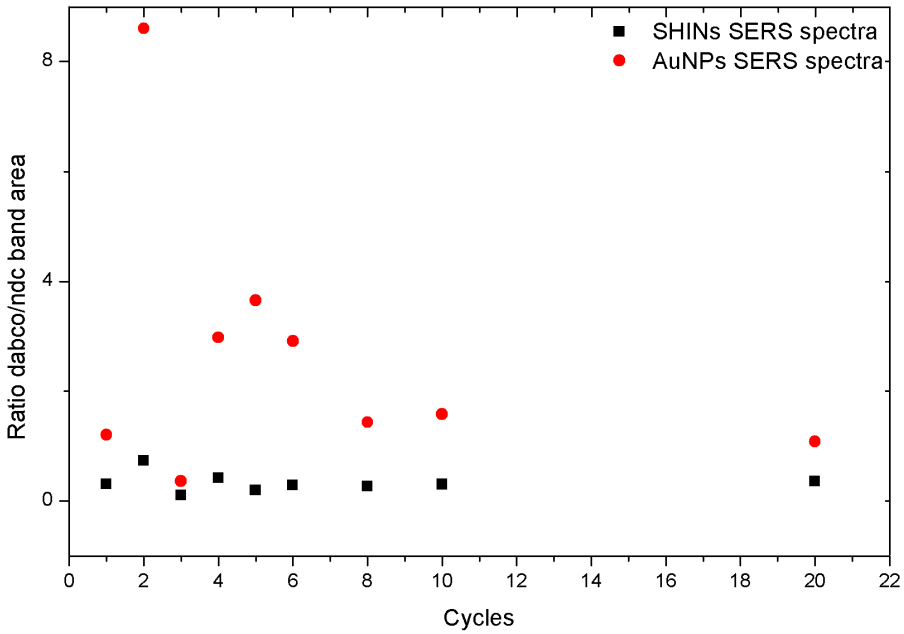

Figure 32: Ratio of the dabco and ndc band areas plotted for the gold nanoparticles and SHIN SERS measurements.

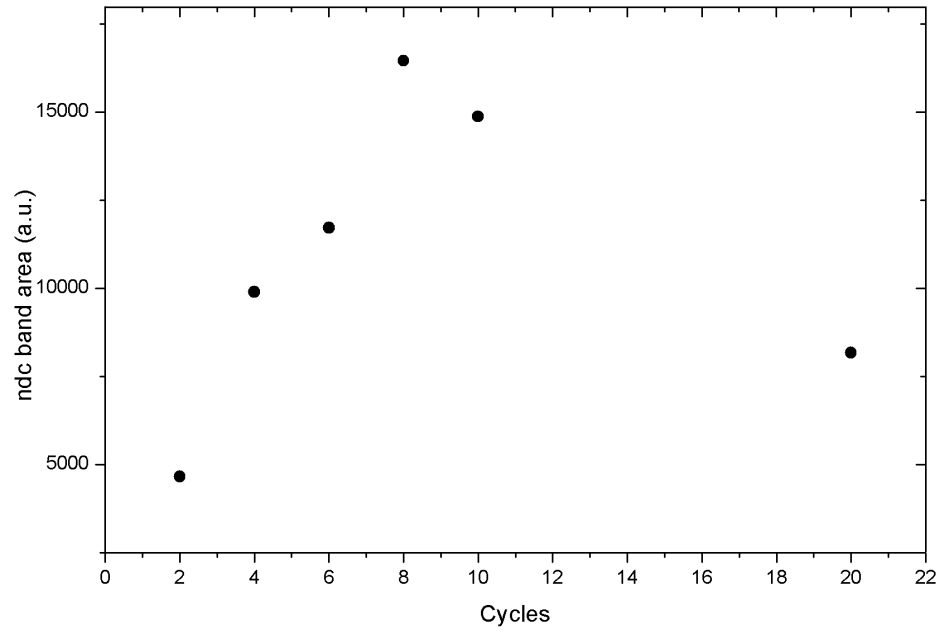

Figure 33: Peak area of the ndc band at 1358 is plotted against the amount of immersion cycles of the SURMOF. As can be seen the amount of SURMOF increases on the substrate. Only measurement 20 deviates from this trend.

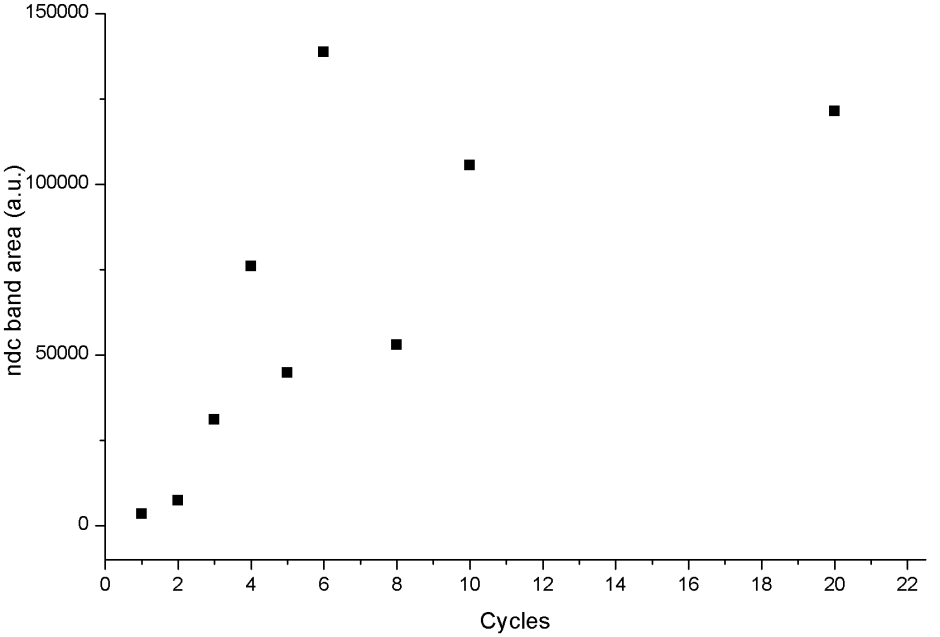

Figure 34: Band area of the ndc band at 1360 cm^{-1} is plotted against the amount of immersion cycles of the SURMOF. As can be seen the amount of SURMOF increases on the substrate.

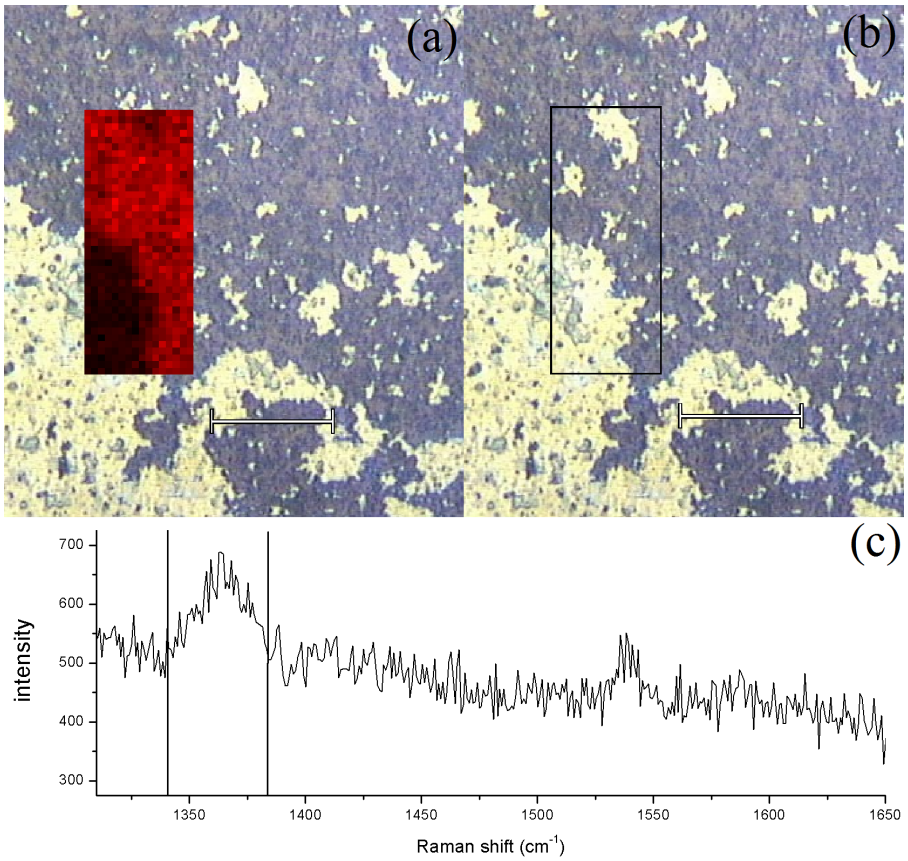

Figure 35: Raman map of the 1 cycle SURMOF sample.(a) shows the image with Raman map. In (b) the area were the Raman map was taken is outlined. (c) shows a typical spectrum of a bright red pixel with the integration limits. As can be seen in the figure already one monolayer of MOF can be detected using SHINs as signal enhancer. The maps were measured using the 785 nm laser at 5% laser intensity. It should be mentioned that this 5% laser intensity is now spread out over a line of a few µm long resulting in an intensity per area lower than used in the point spectra. The scale bar is 20 µm, one pixel of theRaman map is approximately 1 x 1µm.

2, and 5 are shown as examples. The other maps can be found in appendix H. In figure 35 a chemical map of the 1 cycle sample is shown.

On the 1 cycle SURMOF sample we measured 3 Raman maps and in all these measurements the band at 1362 cm^{-1} was visible when there were SHINs on the sample. So it seems that from the Raman map measurements we can conclude that even after one cylce the substrate is covered with some SURMOF. However, we can not say how much MOF layers there are on the substrate. Furthermore a pixel in the chemical map is approximately 1 µm x 1 µm. Within this rather big detection area there could still be islands of MOF with empty substrate in between. However, we can rule out, the existence of big areas of uncoated substrate within our measured areas where SERS particles were present.

In figure 36 and 37 the Raman maps of the 2 and 5 cycles SURMOF samples are shown. The results were very similar to the 1 cycle SURMOF sample. Wherever particles are located the naphthalene C=C stretch vibration at 1362 cm^{-1} was visible. Without particles it was impossible to observe the MOF vibrations. Furthermore there was a slight increase in average peak intensity probably due to more SURMOF being deposited on the substrate.

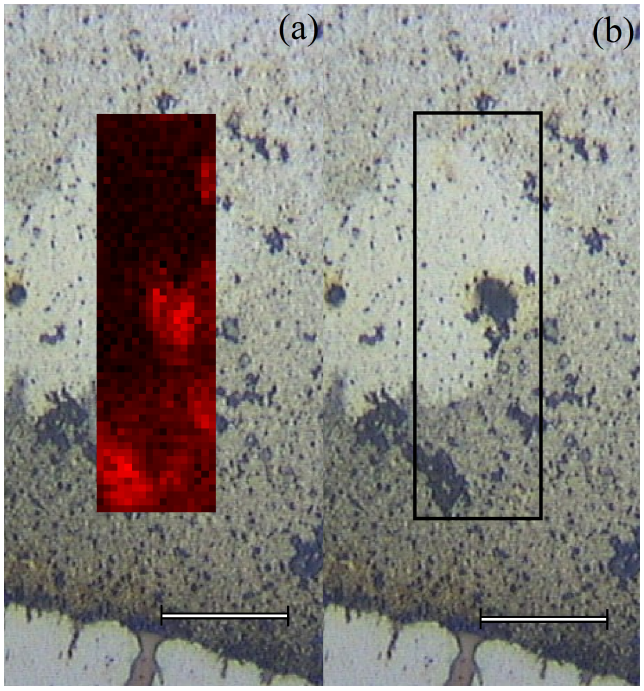

Figure 36: Raman map of the 2 cycles SURMOF sample.(a) shows the image with Raman map. In (b) the area were the Raman map was taken is outlined. The map was measured using the 785 nm laser at 5% laser intensity. The scale bar is 20 µm, one pixel of the Raman map is approximately 1 μm^2. As can be seen there seems to be a good overlap between the Raman map and the position of the particle aggregates which appear as black spots on the optical image.

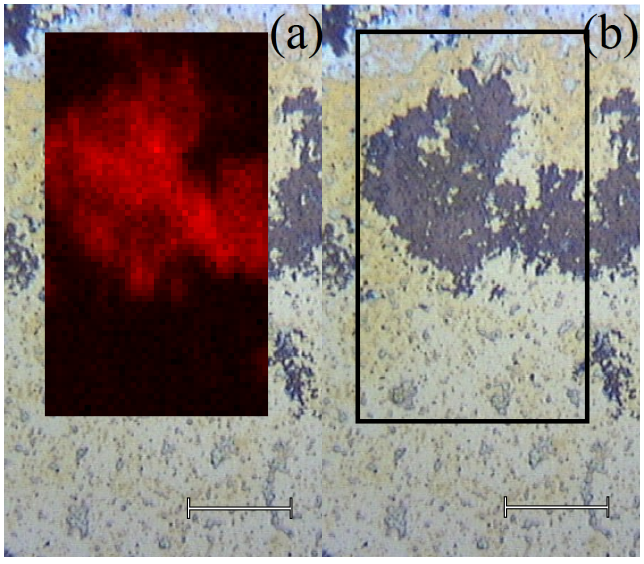

Figure 37: Raman map of the 5 cycles SURMOF sample.(a) shows the image with Raman map. In (b) the area were the Raman map was taken is outlined. The map was measured using the 785 nm laser at 5% laser intensity. The scale bar is 20 µm, one pixel of the Raman map is approximately 1 μm^2.

4.2.7 Averaged Raman maps

To further analyse the raman maps the average spectrum was calculated. Only the datapoints containing the actual MOF spectrum were included, all datapoints without MOF bands (dark) were excluded. This was done by using a mathlab script which discards all datapoints containing no MOF vibrations. In figure 38 the averaged Raman spectra are shown . The 1600 cm^{-1} band shows an clear increase in intensity with increasing deposition cycle. The differnt bands observed were integrated and plotted against the amount of deposition cycles, as shown in figure 38(a), (b) and (c) respectively.

Interestingly, we also see a band at 1454 cm^{-1}, this band could corrospond to the dabco vibration at 1456 cm^{-1} in figure 27. This band was not observed in any of the other Raman spectra. So by averaging the Raman maps the noise in the spectra is reduced resulting in better spectra enabling us to see weaker vibrations.

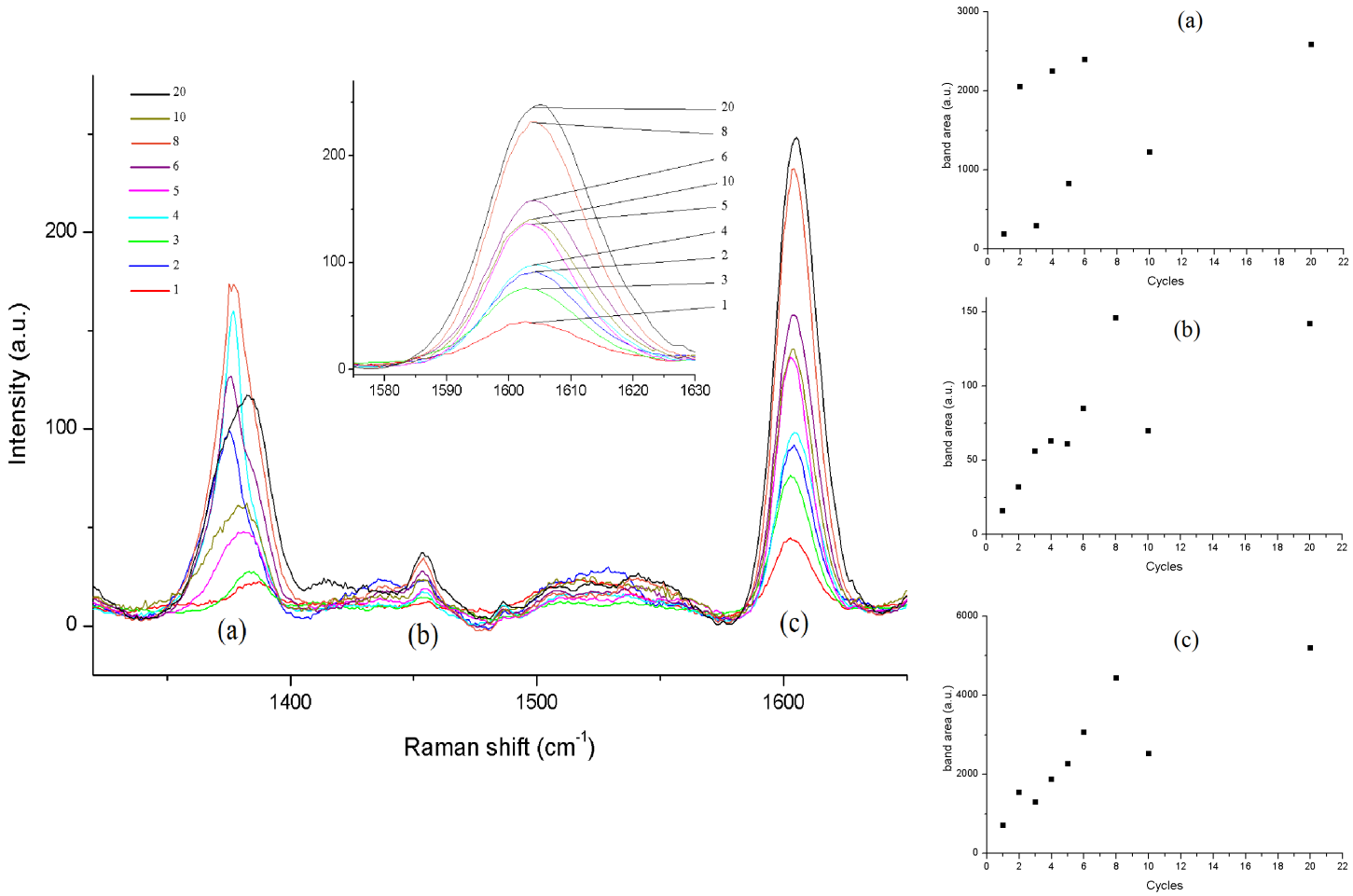

Figure 38: Averaged Raman spectra of the different maps plotted in one figure. The inset shows the 1600 cm^{-1} band magnified. (a), (b) and (c) are the integration data of the different bands plotted against the amount of cycles. As can be seen the general trend observed is an increase in band area per cycle.

5 Conclusions

We have presented a successful chemical identification method for studying very thin SURMOF layers. Both gold and silver nanoparticles, with 785 and 532 nm laser light respectively, can be used to study thin layers of SURMOF on a chemical level. Additionally silica coated gold nanoparticles can also be used used to study SURMOFs giving much more consistent spectra.

Gold nanoparticles proved to be less suitable for doing SERS measurement as the results were much more inconsistent. Especially the ndc bands were not always visible in the gold nanoparticle SERS spectra.

From the quantifications of the SERS spectra we can conclude that it is possible to prove that the MOF thickness increases with subsequent growth cycles. This was visible by the increasing band area of the ndc band at 1360 cm^{-1}. Both with the gold SHINs and the silver nanoparticles this trend was clearly observed.

From the Raman maps we can conclude that even when a single growth cycle was used the entire substrate seemed to be covered with SURMOF. Every pixel in the chemical map which had SHINs on top of it showed the MOF spectrum, however, weakly. The Raman maps of samples with more immersion cycles showed higher intensity of MOF bands, indicating growth.

The AFM images showed that the growth does not proceed in a perfect layer-by-layer fashion, but rather, a nucleation growth type is observed. In this way a corrugated MOF surface is produced. This corrugated surface may contribute to a strong signal.

With the method presented here growth of SURMOFs could be studied. Although techniques such as SPR, QCM and AFM are still preferred when the exact thickness of the SURMOF needs to be probed, this technique has the advantage of supplying the user with more chemical information. For example the gold nanoparticle measurements showed a unexpected dabco-ndc Raman intensity ratio. This was an indication that the sample was structurally damaged, something we would be unable to see in the other techniques mentioned. Another advantage is the low detection limit of this method, this could be used to check the coverage of ultra-thin SURMOFs. Concludingly this method will most likely not be implemented as a standard SURMOF characterization method. However, when chemical information is needed or if the samples are very thin our method has advantages over other characterization methods.

6 Outlook

An important research question that is not fully answered in this study is: does the presented method of measuring SERS spectra leave the SURMOFs intact? We are not sure if the morphology of the SURMOFs changes when the nanoparticles are dropcasted. It might be possible that some MOF components dissolve and precipitate when the droplet dries, since both dabco and copper(II) are soluble in water. As mentioned before MOFs containing fully coordinated metal nodes are usually resistant to water [46,47]. However, studies on water resistance are usually done by measuring water adsorption isotherms on bulk MOFs. Hence, to strengthen the results presented in this study, several experiments could be conducted to investigate the integrity of the SURMOF under our experimental conditions.

First of all to confirm the water resistance of the SURMOF, AFM scans after treatment with water could be investigated. If the morphology and thickness of the area where the water droplet was located is the same as the untreated part of the substrate, evidence is given given for the water resistance of thin layers of this SURMOF. Additionally, AFM could be used to study the morphology of the nanoparticles cast on the SURMOFs. This would also provide more information on the SURMOF integrity under these experimental conditions.

XRD is often used in research on SURMOFs to investigate the degree of crystallinity of the material. However, when very thin SURMOF samples are studied XRD is not usable any more as it relies on interference effects of waves scattered on crystal planes. If only few crystal planes are present, the effect is too weak to observe. So XRD could be used to study the samples with cycles 10-20, but samples with less cycles can most likely not be examined. Consequently, XRD can be used to study the crystallinity of the samples with >10 cycles.

Another possible option to study the directionality of the SURMOF is using polarized light in the Raman measurements. Because the ligands in the MOF are ideally oriented in a certain direction some vibrations will become inactive when the incident light is polarized. So if the Raman spectra look different for different directions of polarization we know that the molecules in the MOF are not oriented randomly. This would also be an indication that the MOF retains its structure. One important side note is that when SERS measurements are done the polarization of the incident light is not fully conserved as the light is 'focused' locally [58,59]. So it might not be possible to use mentioned polarization effects in combination with SERS. However it can be used with normal Raman measurements.

It would be interesting to further explore the possibilities of SERS measurements on MOFs. First of all the deposition method could be changed so a more homogeneous coverage of the SURMOF substrate is achieved. For example a monolayer of SHINs could be deposited on the SURMOF using a modified Langmuir-Blodgett method [60,61]. By adsorbing the SHINs on a liquid-air interface, a monolayer of particles can be formed. If a SURMOF substrate is immersed in the liquid, and pulled vertically from the film with constant speed a monolayer of SHINs is deposited on the substrate. With AFM or SEM the coverage and morphology of these particle monolayers could be imaged. A drawback is the introduction of more components such as solvents in the system. The big advantage is that when measuring SERS on a perfect monolayer of SHINs, quantification of the results is far more straightforward. With this experimental approach the amount of particles is constant in each measurement meaning all parameters can be held constant, except for MOF thickness. This would imply that the MOF band intensity can be directly related to the SURMOF thickness.

Lastly, X-ray techniques like EXAFS could be used to study the nature of the copper ions. This would give information about the geometric and electronic structure of the SURMOF and copper ions respectively. It should be noted that synchotron beam time would be required to do such experiments.

The use of SERS as a analytic tool for studying SURMOFs or MOFs has not been

reported anywhere before. There are most likely a range of other systems where SERS can be applied to, which are unknown or undiscovered as of now. Especially with the introduction of SHINs, SERS shows great potential as an analytic tool.

In conclusion, it seems that still a lot of research can be done in the field of SURMOFs. A lot of literature has been published on potential applications and properties of MOFs [43,62]. However, far less has been published on growth of mentioned SUFMORs. It is still not fully understood how MOFs nucleate and grow on surfaces, especially SURMOFs. If these potential applications become reality, it is important to understand how this growth works on a molecular level, to improve the performances of such applications.

7 Acknowledgements

I would like to thank Rogier Brand for daily supervision and prof. dr. ir. B.M.Weckhuysen for making it possible to do my master thesis at the Inorganic Chemistry and Cataysis group. Furthermore, I would like to thank Cor van der Spek, Jaco Geuchies and Pasi Paalanen for providing TEM images of the nanoparticles.

Appendix A Additional TEM data

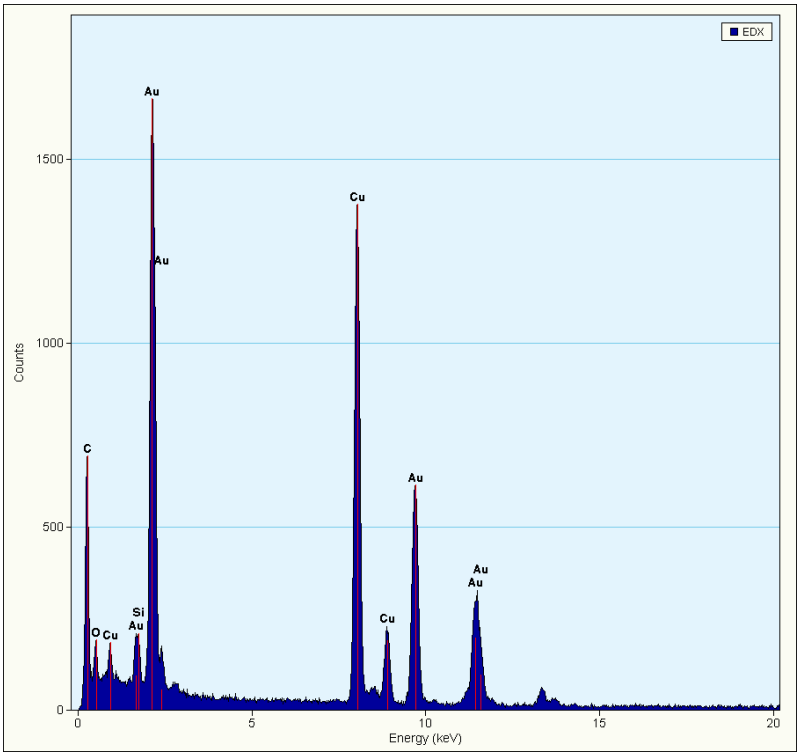

Figure 39: EDX of the SHINs. The copper peak originates from the TEM grid, the carbon peak originates from the carbon film on the TEM grid. Gold, silicon and oxygen peaks are observed, indicating that silica has been deposited on the gold nanoparticles.

Appendix B Copper acetate Raman spectrum

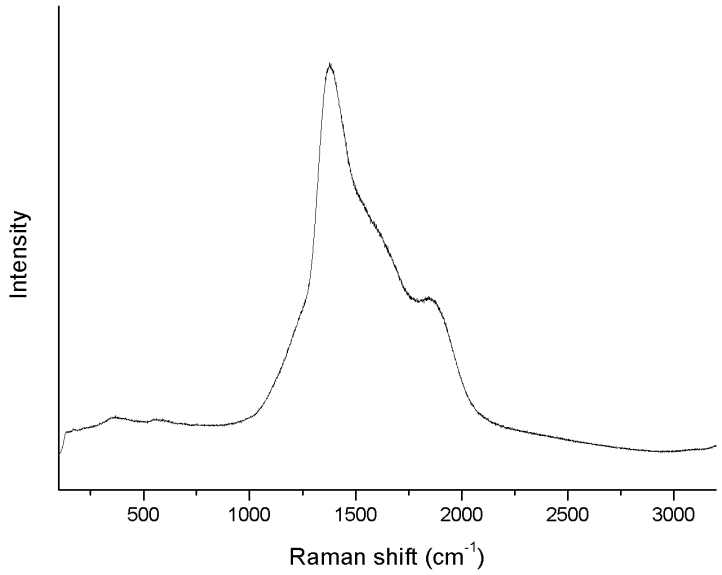

Figure 40: Raman spectrum of copper(II) acetate measured with 785 nm at 5% laser power, 50x objective, 10 seconds exposer time. Only a big fluoresence band is observed, it was impossible to observe vibrations.

Appendix C Gold nanoparticles and SHIN blanco SERS measurement

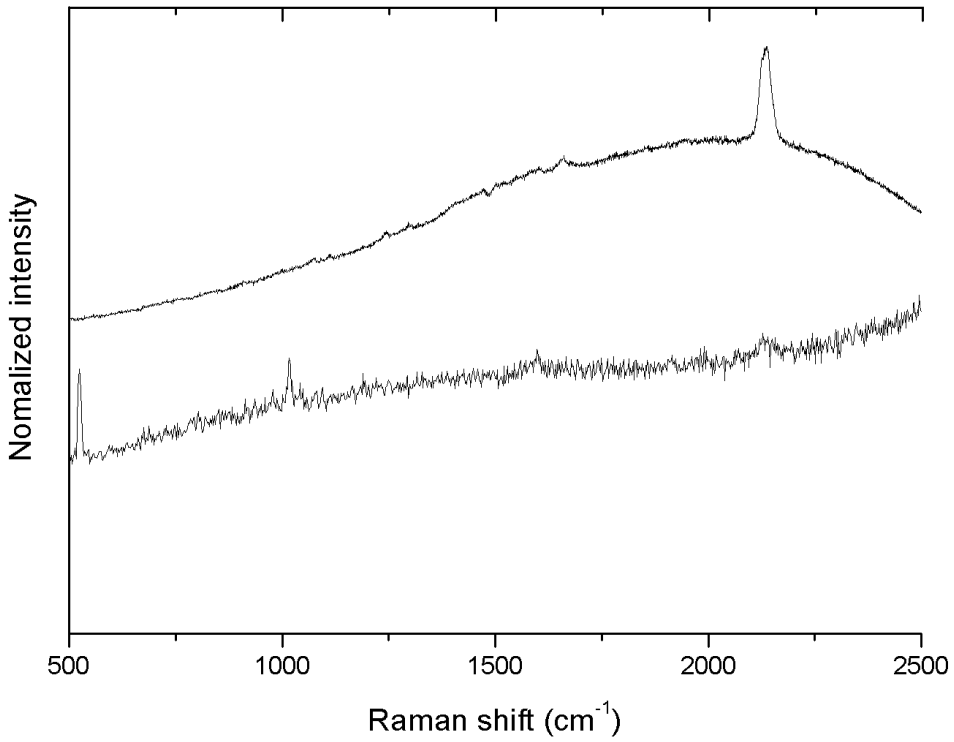

Figure 41: Raman spectra of the gold nanoparticles and SHINSs(top and bottom respectively) on a silicon wafer measured with 785 nm at o.1% laser power, NA 0.75 spotsize 0.52µm, power $2.97 \cdot 10^{-3}$ W cm^{-1}, 50x objective, 10 seconds exposure time. As can be ssen the gold nanoparticle spectrum shows a band at 213 8^{-1} indicative of citrate, this band is almost invisable in the SHIN spectrum the SHIN spectrum shows the silicon vibration at 520 cm^{-1}. This vibration is not observed in the gold nanoparticle spectrum, probably because more particles were present in this measurement.

Appendix D Optical images of the samples

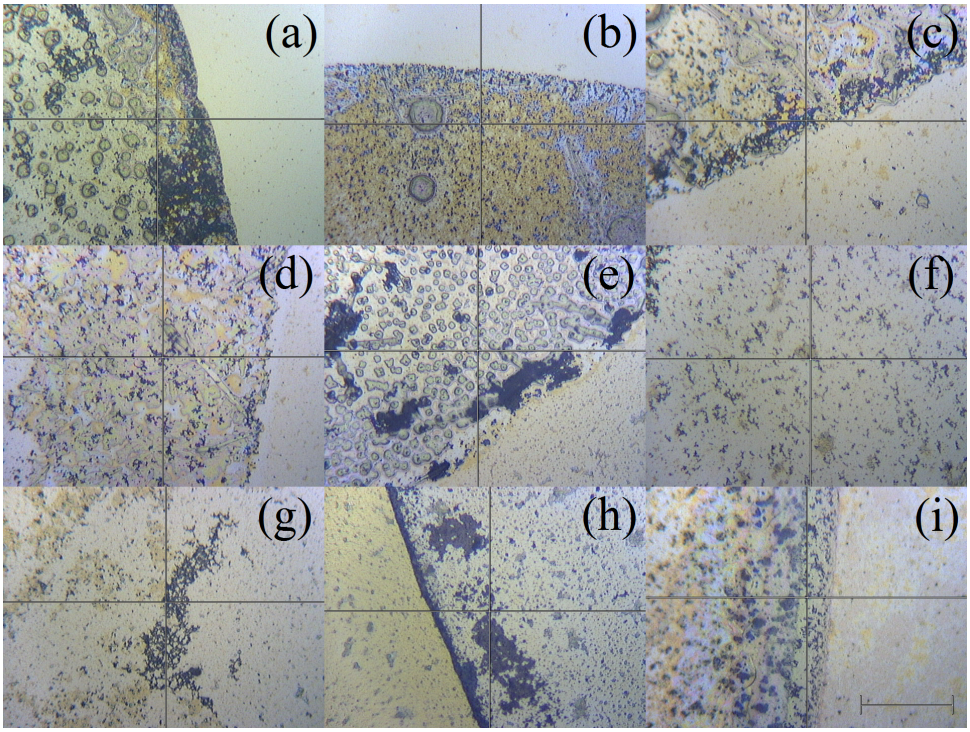

Figure 42: Optical images of the gold nanoparticles dropcasted on the substrates, (a)...(i) corrospond to substrates with cycles 1.... 20 respectively. The crosshair indicates the position were the laser beam was positioned, as can be seen the crosshair is always on a black spot containing the gold nanoparticles. If the beam was pointed next to the droplet no signal was obtained. Proving that the SERS effect is needed to observe the MOF bands. It was also found that if the the beam was positioned on the middle of a dark area no signal was obtained, in this case probably too much particles are on the substrate blocking the light from reaching the MOF.

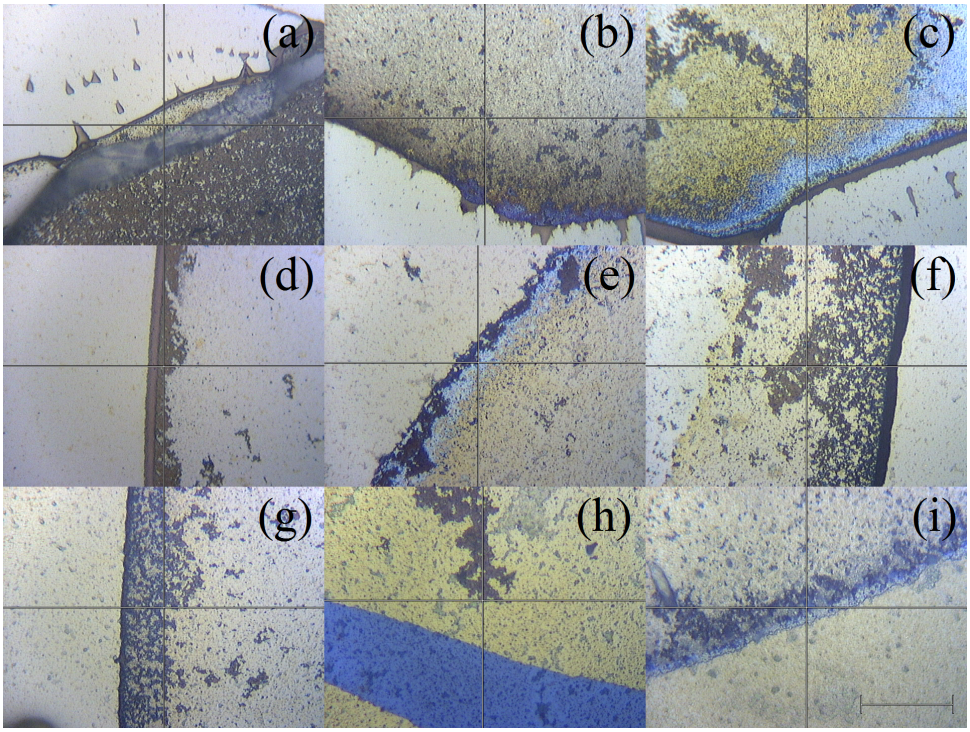

Figure 43: Optical images of the SHINs dropcasted on the substrates, (a)...(i) corrospond to substrates with cycles 1...20 respectively. The crosshair indicates the position were the laser beam was positioned, as can be seen the crosshair is always on a black spot containing the SHINs.

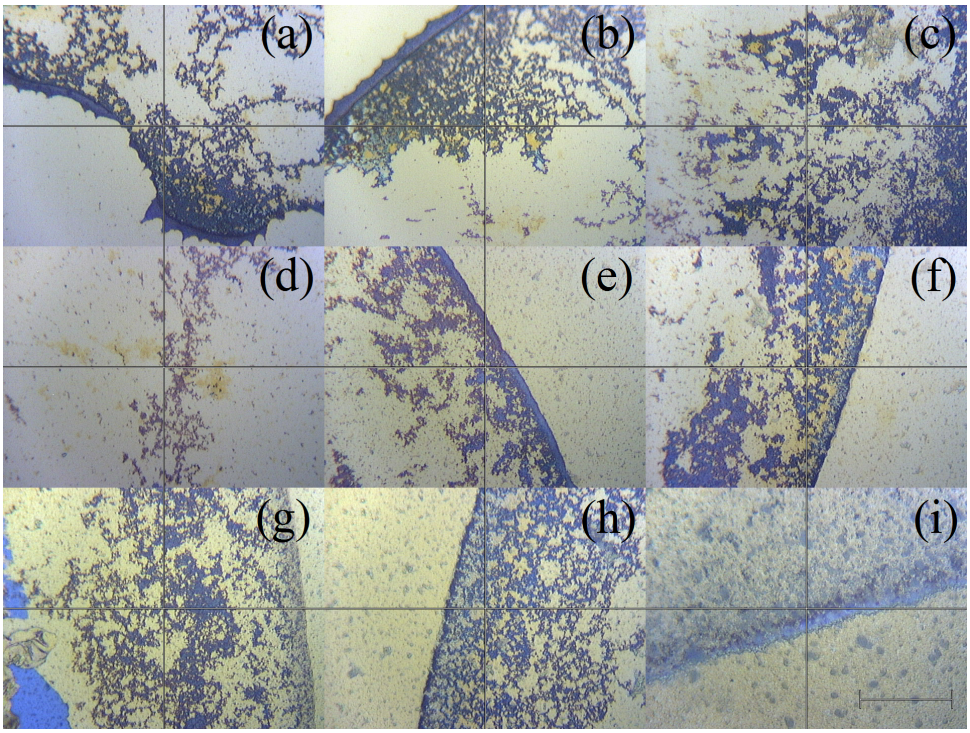

Figure 44: Optical images of the silver nanoparticles dropcasted on the substrates, (a)...(i) corrospond to substrates with cycles 1...20 respectively. The crosshair indicates the position were the laser beam was positioned, as can be seen the crosshair is always on a black spot containing the silver nanoparticles. It was found that if the the beam was positioned on the middle of a dark area no signal was obtained, in this case probably too much particles are on the substrate blocking al the light from the sample.

Appendix E SHIN SERS spectra: entire region

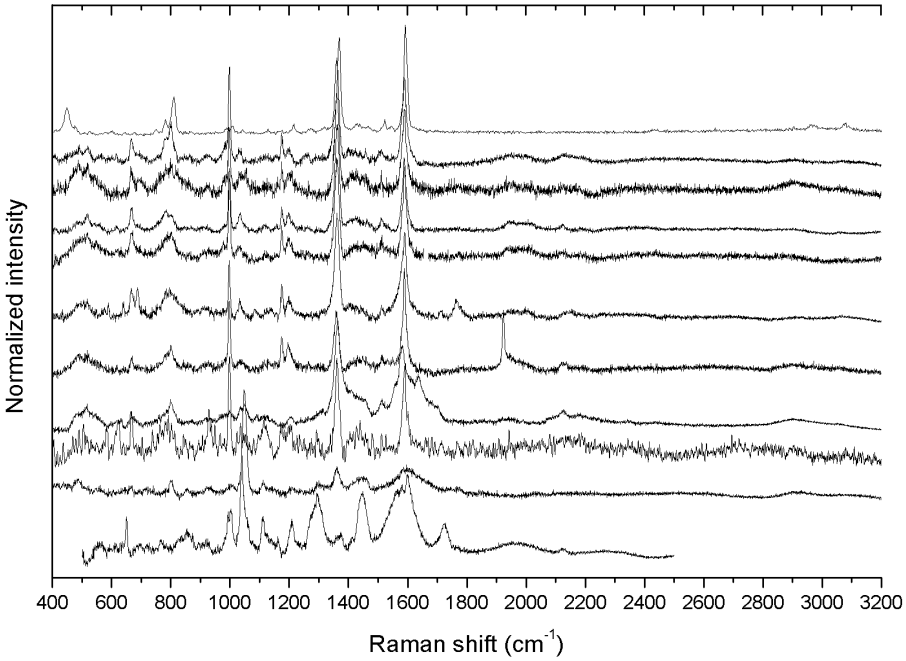

Figure 45: Raman spectra of all Cu(ndc)(dabco)$_{0.5}$ samples measured with SHINs. The top spectrum is not a SERS measurement but just a regular Raman measurement of bulk Cu(ndc)(dabco)$_{0.5}$. The SERS measurements were all performed with a 785 nm laser operating at 0.05% laser power, NA 0.75, spotsize 0.52µm, power $1.39 \cdot 10^3$ W cm^{-1} . A 50x objective was used with a 1200 l/mm grating. The exposure time was 10 seconds, the amount of accumulations varied from 1 to 4 depending on the quality of the spectrum. As can be seen in the figure no citrate band is visible.

Appendix F Original SERS spectra

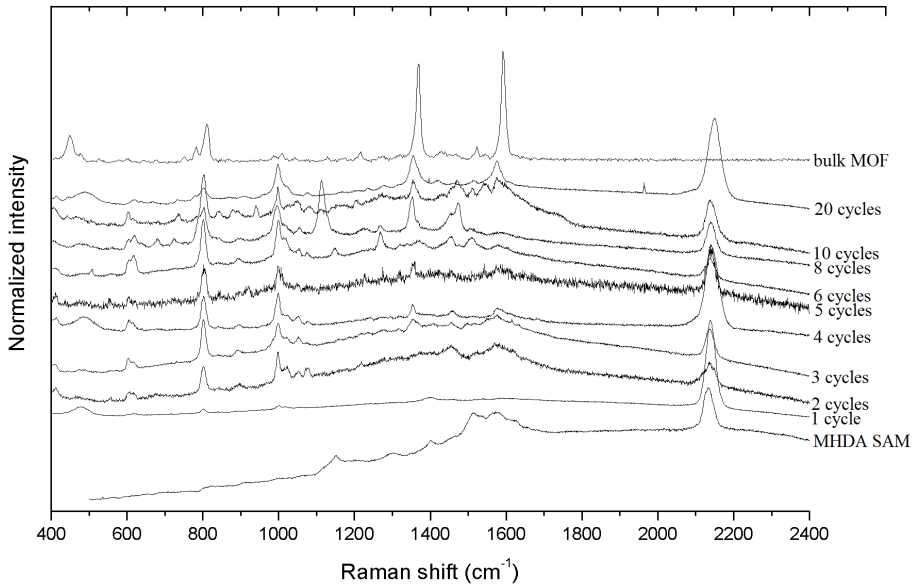

Figure 46: Raman spectra of all $Cu(ndc)(dabco)_{0.5}$ samples measured with gold nanoparticles. The SERS measurements were all performed with a 785 nm laser operating at 0.05% laser power. A 50x objective was used with a 1200 l/mm grating. The exposure time was 10 seconds, the amount of accumulations varied from 3 to 5 depending on the quality of the spectrum.

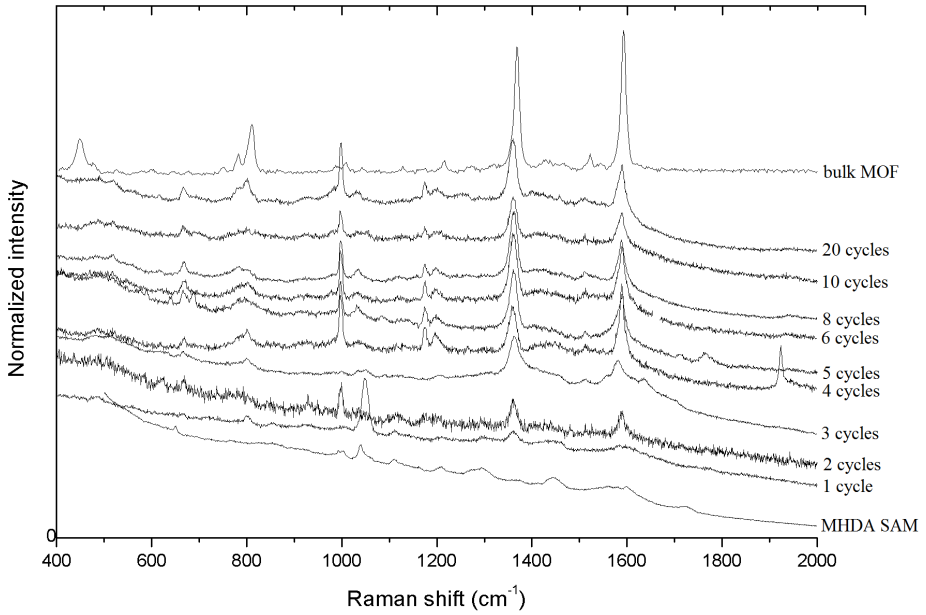

Figure 47: Raman spectra of all Cu(ndc)(dabco)$_{0.5}$ samples measured with SHINs. The top spectrum is not a SERS measurement but just a regular Raman measurement of bulk Cu(ndc)(dabco)$_{0.5}$. The SERS measurements were all performed with a 785 nm laser operating at 0.05% laser power. A 50x objective was used with a 1200 l/mm grating. The exposure time was 10 seconds, the amount of accumulations varied from 1 to 4 depending on the quality of the spectrum.

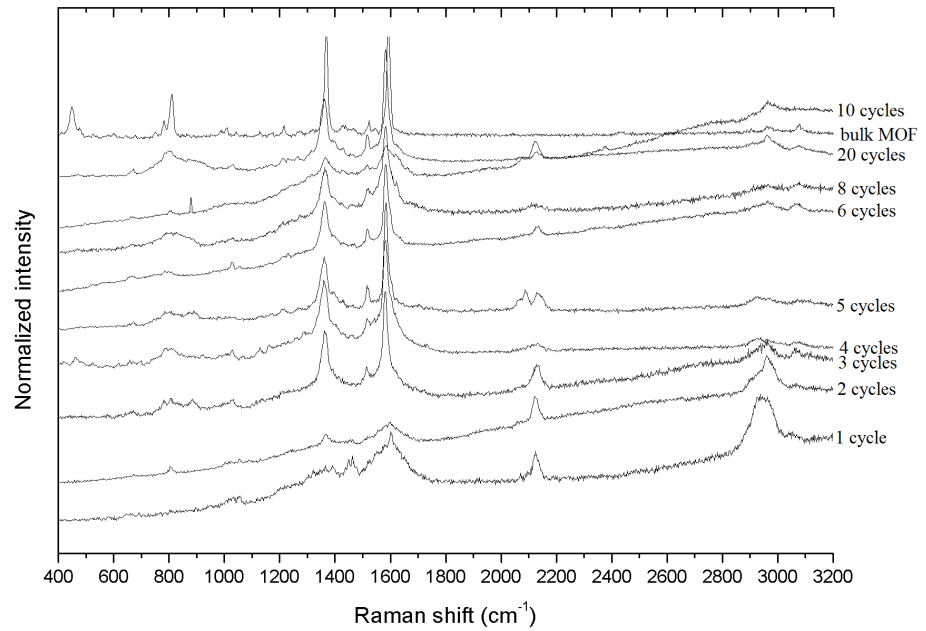

Figure 48: Raman spectra of all Cu(ndc)(dabco)$_{0.5}$ samples measured with silver nanoparticle The top spectrum is not a SERS measurement but just a regular Raman measurement of bulk Cu(ndc)(dabco)$_{0.5}$. The SERS measurements were all performed with a 532 nm laser operating at 0.05% laser power. A 50x objective was used with a 1200 l/mm grating. The exposure time was 10 seconds and the amount of accumulations was one.

Appendix G SERS sensitivity

A rough estimation of the amount of ndc detected can be made. A unit cell of Cu(ndc)(dabco)$_{0.5}$ is approximately 10.8Å by 9.6Å [6]. Assuming we have a perfect monolayer coverage, which is probably an overestimation, we have a concentration of ndc on the surface of: 2 ndc molecules per $10.8 \cdot 9.6 \approx 100 \mathring{A}^2$. 2ndc per $100 \mathring{A}^2 \cdot \frac{10^{-16} cm^2}{\mathring{A}^2} =$ 2ndc per $1.0 \cdot 10^{-14} cm^2$. Per square centimeter that is $2 \cdot 10^{14}$ ndc per cm^2. Dividing by Avogadro's number we get: $2 \cdot 10^{14} \cdot 6.0 \cdot 10^{-23} \approx 3 \cdot 10^{-10} \frac{mol\ ndc}{cm^2}$. This means we have been able to detect 20 nanomol per centimeter, this demonstrates the sensitivity of SERS.

Appendix H Raman maps

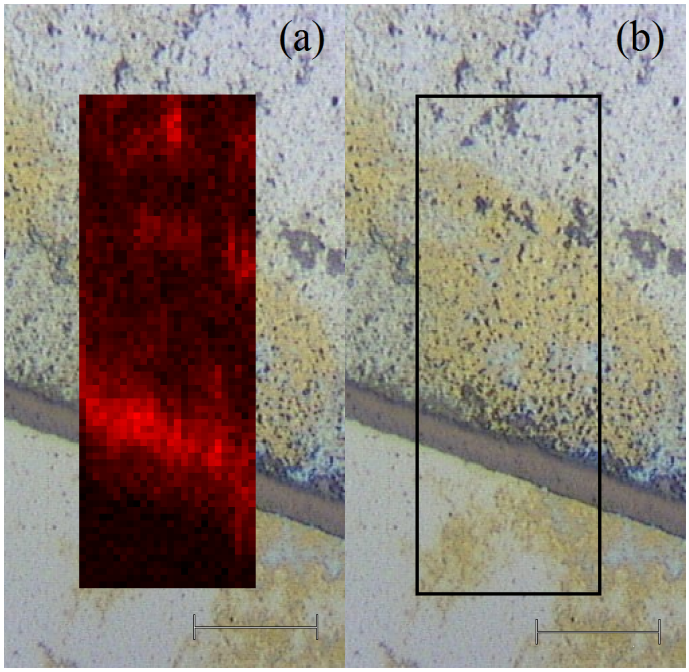

Figure 49: Raman map of the 3 cycle SURMOF sample.

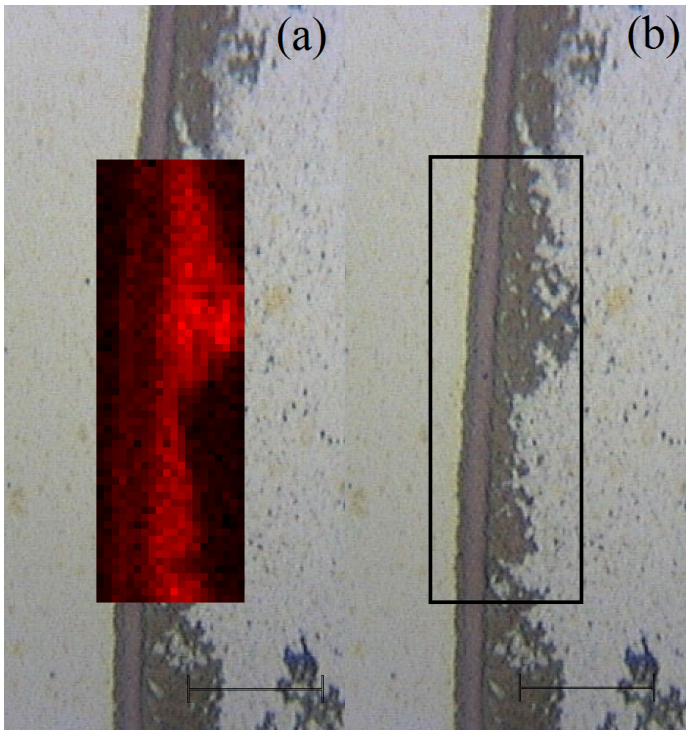

Figure 50: Raman map of the 4 cycle SURMOF sample.

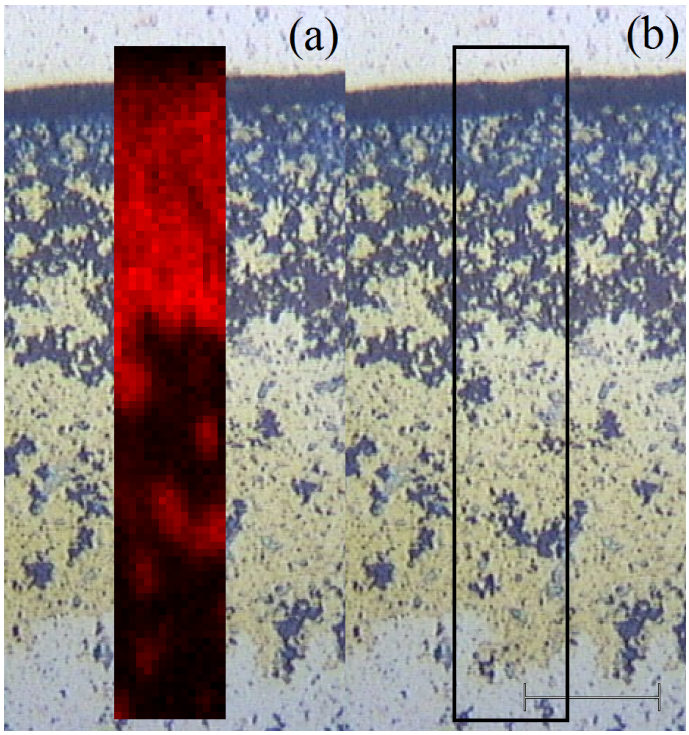

Figure 51: Raman map of the 6 cycle SURMOF sample.

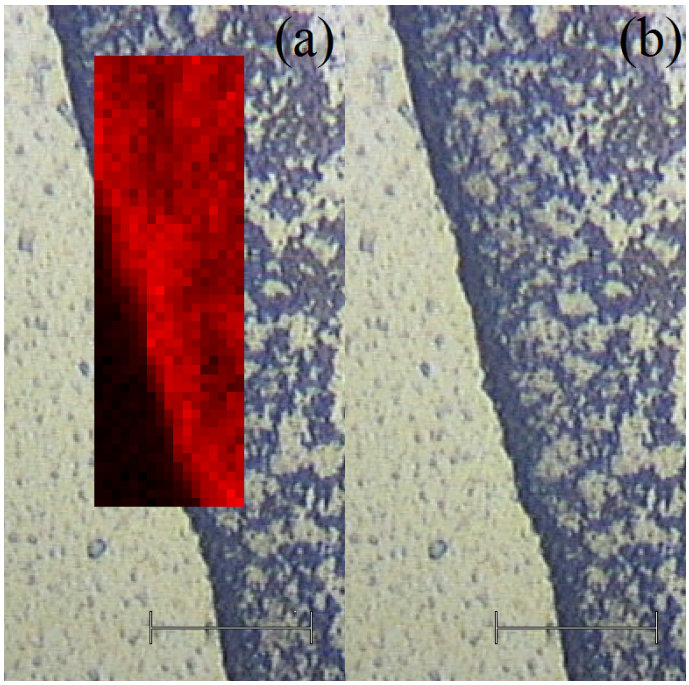

Figure 52: Raman map of the 8 cycle SURMOF sample.

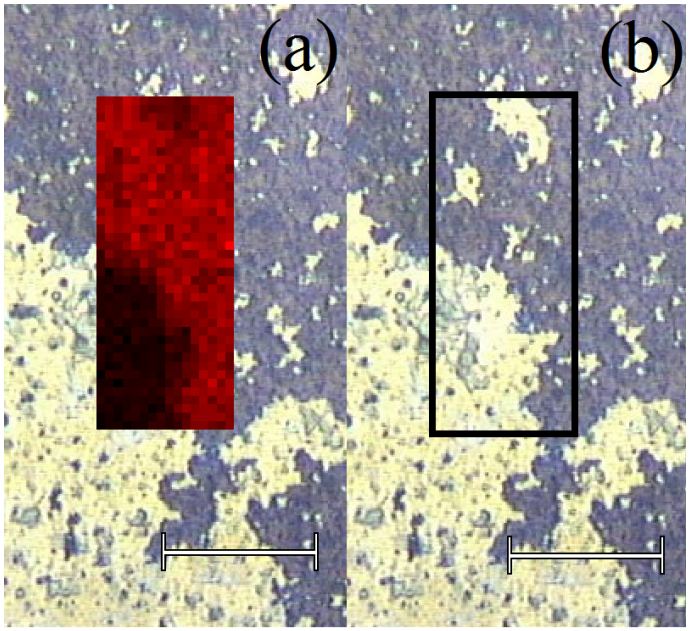

Figure 53: Raman map of the 10 cycle SURMOF sample.

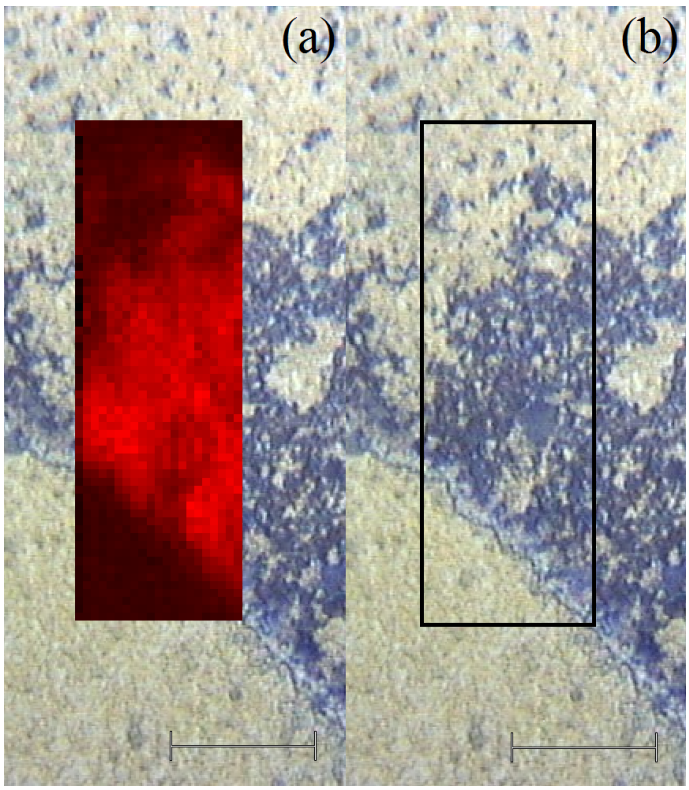

Figure 54: Raman map of the 20 cycle SURMOF sample.

References

[1] A. Campion and P. Kambhampati, "Surface-enhanced Raman scattering," *Chem. Soc. Rev.*, vol. 27, no. 4, pp. 241–250, 1998.

[2] M. G. Albrecht and J. A. Creighton, "Anomalously intense Raman spectra of pyridine at a silver electrode," *Journal of the American Chemical Society*, vol. 99, no. 15, pp. 5215–5217, 1977.

[3] P. L. Stiles, J. A. Dieringer, N. C. Shah, and R. P. Van Duyne, "Surface-enhanced raman spectroscopy," *Annu. Rev. Anal. Chem.*, vol. 1, pp. 601–626, 2008.

[4] J. F. Li, Y. F. Huang, Y. Ding, Z. L. Yang, S. B. Li, X. S. Zhou, F. R. Fan, W. Zhang, Z. Y. Zhou, B. Ren, *et al.*, "Shell-isolated nanoparticle-enhanced Raman spectroscopy," *Nature*, vol. 464, no. 7287, pp. 392–395, 2010.

[5] O. Shekhah, H. Wang, D. Zacher, R. A. Fischer, and C. Wöll, "Growth mechanism of metal–organic frameworks: Insights into the nucleation by employing a step-by-step route," *Angewandte Chemie International Edition*, vol. 48, no. 27, pp. 5038–5041, 2009.

[6] D. Zacher, K. Yusenko, A. Bétard, S. Henke, M. Molon, T. Ladnorg, O. Shekhah, B. Schüpbach, T. de los Arcos, M. Krasnopolski, *et al.*, "Liquid-phase epitaxy of multicomponent layer-based porous coordination polymer thin films of [m (l)$(p)_{0.5}$] type: Importance of deposition sequence on the oriented growth," *Chemistry-a European Journal*, vol. 17, no. 5, pp. 1448–1455, 2011.

[7] T. Ladnorg, A. Welle, S. Heißler, C. Wöll, and H. Gliemann, "Site-selective growth of surface-anchored metal-organic frameworks on self-assembled monolayer patterns prepared by AFM nanografting," *Beilstein journal of nanotechnology*, vol. 4, no. 1, pp. 638–648, 2013.

[8] C. Munuera, O. Shekhah, H. Wang, C. Wöll, and C. Ocal, "The controlled growth of oriented metal–organic frameworks on functionalized surfaces as followed by scanning force microscopy," *Physical Chemistry Chemical Physics*, vol. 10, no. 48, pp. 7257–7261, 2008.

[9] D. W. Ball, *Physical Chemistry*. Chapter 14 Rotational and Vibrational Spectroscopy, Cengage Learning, 2002. pp. 34-66.

[10] J. M. Chalmers, H. G. M. Edwards, and M. D. Hargreaves, *Vibrational Spectroscopy Techniques: Basics and Instrumentation*, pp. 9–44. John Wiley & Sons, Ltd, 2012.

[11] R. Aroca, *Surface-Enhanced Vibrational Spectroscopy*. Chapter 1: Theory of Molecular vibrations. The Origin of Infrared and Raman Spectra, Wiley Publishing, 2006. pp. 8–39.

[12] C. V. Raman and K. S. Krishnan, "A new type of secondary radiation," *Nature*, vol. 121, no. 3048, pp. 501–502, 1928.

[13] C. V. Raman, "A new radiation," *Indian Journal of physics*, vol. 2, pp. 387–398, 1928.

[14] D. Long, *Raman spectroscopy*. McGraw-Hill International Book Company, 1977. pp. 45-61.

[15] M. D. B. Daniel C. Harris, *Symmetry and Spectroscopy: An Introduction to Vibrational and Electronic Spectroscopy*. Dover Publications, 1989. pp. 123–145.

[16] R. Aroca, *Surface-Enhanced Vibrational Spectroscopy.* Chapter 3: Surface-Enhanced Raman Scattering, Wiley Publishing, 2006. pp. 76–101.

[17] A. Otto, "The chemical(electronic) contribution to surface-enhanced raman scattering," *Journal of Raman Spectroscopy*, vol. 36, no. 6-7, pp. 497–509, 2005.

[18] M. Moskovits, *Surface-Enhanced Raman Scattering*, vol. 103 of *Topics in Applied Physics*. Springer Berlin Heidelberg, 2006. pp.1–17.

[19] E. J. Blackie, E. C. L. Ru, and P. G. Etchegoin, "Single-molecule surface-enhanced raman spectroscopy of nonresonant molecules," *Journal of the American Chemical Society*, vol. 131, no. 40, pp. 14466–14472, 2009.

[20] E. Le Ru, E. Blackie, M. Meyer, and P. G. Etchegoin, "Surface enhanced raman scattering enhancement factors: a comprehensive study," *The Journal of Physical Chemistry C*, vol. 111, no. 37, pp. 13794–13803, 2007.

[21] P. E. Eric Le Ru, *Principles of Surface-Enhanced Raman Spectroscopy and related plasmonic effects*. Topics in Applied Physics, Elsevier, 2008. pp. 1–17.

[22] F. Zhou, Z.-Y. Li, Y. Liu, and Y. Xia, "Quantitative analysis of dipole and quadrupole excitation in the surface plasmon resonance of metal nanoparticles," *The Journal of Physical Chemistry C*, vol. 112, no. 51, pp. 20233–20240, 2008.

[23] T. Wang, Z. Zhang, F. Liao, Q. Cai, Y. Li, S.-T. Lee, and M. Shao, "The effect of dielectric constants on noble metal/semiconductor sers enhancement: FDTD simulation and experiment validation of Ag/Ge and Ag/Si substrates," *Scientific reports*, vol. 4, pp. 1–8, 2014.

[24] K. L. Wustholz, A.-I. Henry, J. M. McMahon, R. G. Freeman, N. Valley, M. E. Piotti, M. J. Natan, G. C. Schatz, and R. P. V. Duyne, "Structure- activity relationships in gold nanoparticle dimers and trimers for surface-enhanced raman spectroscopy," *Journal of the American Chemical Society*, vol. 132, no. 31, pp. 10903–10910, 2010.

[25] L. Rodriguez-Lorenzo, R. A. Alvarez-Puebla, F. J. G. de Abajo, and L. M. Liz-Marzán, "Surface enhanced raman scattering using star-shaped gold colloidal nanoparticles," *The Journal of Physical Chemistry C*, vol. 114, no. 16, pp. 7336–7340, 2009.

[26] K. D. Alexander, M. J. Hampton, S. Zhang, A. Dhawan, H. Xu, and R. Lopez, "A high-throughput method for controlled hot-spot fabrication in sers-active gold nanoparticle dimer arrays," *Journal of Raman Spectroscopy*, vol. 40, no. 12, pp. 2171–2175, 2009.

[27] A. Otto, "The chemical(electronic) contribution to surface-enhanced raman scattering," *Journal of Raman Spectroscopy*, vol. 36, no. 6-7, pp. 497–509, 2005.

[28] A. Otto, I. Mrozek, H. Grabhorn, and W. Akemann, "Surface-enhanced raman scattering," *Journal of Physics: Condensed Matter*, vol. 4, no. 5, p. 1143, 1992.

[29] R. Aroca, *Surface-Enhanced Vibrational Spectroscopy.* Chapter 6: SERS/SERRS, the Analytical tool, Wiley Publishing, 2006. pp. 151–173.

[30] G. Frens, "Controlled nucleation for the regulation of the particle size in monodisperse gold suspensions," *Nature*, no. 241, pp. 20–22, 1972.

[31] X. Ji, X. Song, J. Li, Y. Bai, W. Yang, and X. Peng, "Size control of gold nanocrystals in citrate reduction: the third role of citrate," *Journal of the American Chemical Society*, vol. 129, no. 45, pp. 13939–13948, 2007.

[32] P. CooperáStevenson *et al.*, "A study of the nucleation and growth processes in the synthesis of colloidal gold," *Discussions of the Faraday Society*, vol. 11, pp. 55–75, 1951.

[33] N. R. Jana, L. Gearheart, and C. J. Murphy, "Seeding growth for size control of 5-40 nm diameter gold nanoparticles," *Langmuir*, vol. 17, no. 22, pp. 6782–6786, 2001.

[34] P. Lee and D. Meisel, "Adsorption and surface-enhanced raman of dyes on silver and gold sols," *The Journal of Physical Chemistry*, vol. 86, no. 17, pp. 3391–3395, 1982.

[35] V. Uzayisenga, X.-D. Lin, L.-M. Li, J. R. Anema, Z.-L. Yang, Y.-F. Huang, H.-X. Lin, S.-B. Li, J.-F. Li, and Z.-Q. Tian, "Synthesis, characterization, and 3D-FDTD simulation of Ag@ Sio2 nanoparticles for ieeetr-enhanced Raman spectroscopy," *Langmuir*, vol. 28, no. 24, pp. 9140–9146, 2012.

[36] L. M. Liz-Marzán, M. Giersig, and P. Mulvaney, "Homogeneous silica coating of vitreophobic colloids," *Chemical communications*, no. 6, pp. 731–732, 1996.

[37] J. F. Li, X. D. Tian, S. B. Li, J. R. Anema, Z. L. Yang, Y. Ding, Y. F. Wu, Y. M. Zeng, Q. Z. Chen, B. Ren, *et al.*, "Surface analysis using shell-isolated nanoparticle-enhanced raman spectroscopy," *nature protocols*, vol. 8, no. 1, pp. 52–65, 2013.

[38] H.-H. Perkampus, H.-C. Grinter, and T. Threlfall, *UV-VIS Spectroscopy and its Applications*. Springer, 1992. pp. 23-55.

[39] L. Reimer and H. Kohl, *Transmission electron microscopy: physics of image formation*, vol. 36. Springer Science & Business Media, 2008. pp. 56-90.

[40] G. Haugstad, *Atomic force microscopy: understanding basic modes and advanced applications*. John Wiley & Sons, 2012. pp. 44-79.

[41] J. R. Long and O. M. Yaghi, "The pervasive chemistry of metal–organic frameworks," *Chemical Society Reviews*, vol. 38, no. 5, pp. 1213–1214, 2009.

[42] D. Zacher, O. Shekhah, C. Wöll, and R. A. Fischer, "Thin films of metal–organic frameworks," *Chemical Society Reviews*, vol. 38, no. 5, pp. 1418–1429, 2009.

[43] O. Shekhah, J. Liu, R. Fischer, and C. Wöll, "MOF thin films: existing and future applications," *Chemical Society Reviews*, vol. 40, no. 2, pp. 1081–1106, 2011.

[44] O. Shekhah, H. Wang, S. Kowarik, F. Schreiber, M. Paulus, M. Tolan, C. Sternemann, F. Evers, D. Zacher, R. A. Fischer, *et al.*, "Step-by-step route for the synthesis of metal-organic frameworks," *Journal of the American Chemical Society*, vol. 129, no. 49, pp. 15118–15119, 2007.

[45] P. Küsgens, M. Rose, I. Senkovska, H. Fröde, A. Henschel, S. Siegle, and S. Kaskel, "Characterization of metal-organic frameworks by water adsorption," *Microporous and Mesoporous Materials*, vol. 120, no. 3, pp. 325–330, 2009.

[46] P. M. Schoenecker, C. G. Carson, H. Jasuja, C. J. Flemming, and K. S. Walton, "Effect of water adsorption on retention of structure and surface area of metal–organic frameworks," *Industrial & Engineering Chemistry Research*, vol. 51, no. 18, pp. 6513–6519, 2012.

[47] N. C. Burtch, H. Jasuja, and K. S. Walton, "Water stability and adsorption in metal–organic frameworks," *Chemical reviews*, vol. 114, no. 20, pp. 10575–10612, 2014.

[48] Z. Liang, M. Marshall, and A. L. Chaffee, "CO_2 adsorption, selectivity and water tolerance of pillared-layer metal organic frameworks," *Microporous and Mesoporous Materials*, vol. 132, no. 3, pp. 305–310, 2010.

[49] S. Link and M. A. El-Sayed, "Size and temperature dependence of the plasmon absorption of colloidal gold nanoparticles," *The Journal of Physical Chemistry B*, vol. 103, no. 21, pp. 4212–4217, 1999.

[50] J. Rodríguez-Fernández, I. Pastoriza-Santos, J. Perez-Juste, F. J. García de Abajo, and L. M. Liz-Marzan, "The effect of silica coating on the optical response of sub-micrometer gold spheres," *The Journal of Physical Chemistry C*, vol. 111, no. 36, pp. 13361–13366, 2007.

[51] D. Irish, D. Guzonas, and G. Atkinson, "Surface enhanced raman spectroscopy of the silver/KCl, triethylenediamine (dabco), water system," *Surface Science*, vol. 158, no. 1, pp. 314–324, 1985.

[52] G. Socrates, *Infrared and Raman characteristic group frequencies: tables and charts*. John Wiley & Sons, 2004. pp. 20–180.

[53] D. A. Guzonas and D. E. Irish, "A raman and infrared spectroscopic study of triethylenediamine (dabco) and its protonated forms," *Canadian journal of chemistry*, vol. 66, no. 5, pp. 1249–1257, 1988.

[54] M. Govindarajan, K. Ganasan, S. FLPeriandy, and M. Karabacak, "Experimental (FT-IR and FT-Raman), electronic structure and DFT studies on 1-methoxynaphthalene," *Spectrochimica Acta Part A: Molecular and Biomolecular Spectroscopy*, vol. 79, no. 3, pp. 646–653, 2011.

[55] C. Prestipino, L. Regli, J. Vitillo, F. Bonino, A. Damin, C. Lamberti, A. Zecchina, P. Solari, K. Kongshaug, and S. Bordiga, "Local structure of framework Cu (II) in HKUST-1 metallorganic framework: spectroscopic characterization upon activation and interaction with adsorbates," *Chemistry of materials*, vol. 18, no. 5, pp. 1337–1346, 2006.

[56] I. Ojea-Jiménez, F. M. Romero, N. G. Bastús, and V. Puntes, "Small gold nanoparticles synthesized with sodium citrate and heavy water: insights into the reaction mechanism," *The Journal of Physical Chemistry C*, vol. 114, no. 4, pp. 1800–1804, 2010.

[57] M. Mabuchi, T. Takenaka, Y. Fujiyoshi, and N. Uyeda, "Surface enhanced Raman scattering of citrate ions adsorbed on gold sol particles," *Surface Science*, vol. 119, no. 2, pp. 150–158, 1982.

[58] P. G. Etchegoin, C. Galloway, and E. Le Ru, "Polarization-dependent effects in surface-enhanced raman scattering (SERS)," *Physical Chemistry Chemical Physics*, vol. 8, no. 22, pp. 2624–2628, 2006.

[59] H. Xu and M. Käll, "Polarization-dependent surface-enhanced Raman spectroscopy of isolated silver nanoaggregates," *ChemPhysChem*, vol. 4, no. 9, pp. 1001–1005, 2003.

[60] M. Szekeres, O. Kamalin, R. A. Schoonheydt, K. Wostyn, K. Clays, A. Persoons, and I. Dékány, "Ordering and optical properties of monolayers and multilayers of silica spheres deposited by the langmuir–blodgett method," *Journal of Materials Chemistry*, vol. 12, no. 11, pp. 3268–3274, 2002.

[61] M. Szekeres, O. Kamalin, P. Grobet, R. Schoonheydt, K. Wostyn, K. Clays, A. Persoons, and I. Dékány, "Two-dimensional ordering of stöber silica particles at the air/water interface," *Colloids and Surfaces A: Physicochemical and Engineering Aspects*, vol. 227, no. 1, pp. 77–83, 2003.

[62] R. J. Kuppler, D. J. Timmons, Q.-R. Fang, J.-R. Li, T. A. Makal, M. D. Young, D. Yuan, D. Zhao, W. Zhuang, and H.-C. Zhou, "Potential applications of metal-organic frameworks," *Coordination Chemistry Reviews*, vol. 253, no. 23, pp. 3042–3066, 2009.